Task Report

Bending-Strain Test Results of ITER Nb$_3$Sn Wires and Preliminary Model Analysis

Makoto Takayasu, Luisa Chiesa, Joel H. Schultz, and
Joseph V. Minervini

July 23, 2008

Plasma Science and Fusion Center
Massachusetts Institute of Technology
Cambridge MA 02139 USA

Abstract

Bending effects on Nb_3Sn wires have been investigated to understand the critical current degradation of large Nb_3Sn superconducting cables, such as the ITER conductors. Characterizations of the critical currents of various Nb_3Sn wires were carried out by a previously reported pure-bending strand test device using the 20 T, 195 mm Bitter magnet at the National High Magnetic Field Laboratory. The critical currents were measured over a large range of bending, up to 0.8% of the nominal bending strain at the wire surface. Irreversible degradations of the critical currents due to bending were also evaluated after straightening. Five different Nb_3Sn wires were tested. Three of them were internal-tin wires of recent ITER TF US Oxford and Luvata wires and older EU EM-LMI wire, while two of them were a recent EU EAS and an older Furukawa bronze wire. The experimental data were evaluated with a newly developed integrated model that accounts for neutral axis shift, current transfer length, mechanical filament breakage and uniaxial strain release due to applying bending.

Contents

1. Introduction

Bending effects on Nb_3Sn wires have been investigated to understand the critical current degradation of large Nb_3Sn superconducting cables, such as the ITER conductors. Characterizations of the critical currents of various Nb_3Sn wires were carried out by a previously reported variable pure-bending strand test device using the 20 T, 195 mm Bitter magnet at the National High Magnetic Field Laboratory (NHMFL) [1]-[3]. The critical currents were measured over a wide range of bending, up to 0.8% of the nominal bending strain at the wire surface. Irreversible degradation of the critical currents due to bending was also evaluated after straightening the wire. Five different Nb_3Sn wires, developed by the ITER parties, were tested. Three of them were internal-tin wires of ITER TF US Oxford and Luvata wires and older European (EU) EM-LMI wire, while two of them were a EU European Advanced Superconductors (EAS) and an older Furukawa bronze wire. The relations of the measured pure-bending critical currents to the existing uniaxial strain data of the wires are discussed. The experimental data were evaluated with a newly developed integrated model that accounts for neutral axis shift, current transfer length, mechanical filament breakage and uniaxial strain release due to applying bending. The test results of the five wires can be understood by including these phenomena; however, further studies of mechanical properties of superconducting wires under pure bending are required. The parameters of the critical current scaling law for the exact tested wires have not yet been established. The parameters used for the present analysis are not definitive; however, the resulted model analyses should not be affected by slight changes of the parameters.

2. Test Method

The bending tests were carried out using our variable bending test device developed and described earlier [1]-[3]. The device can apply a large range of bending, in liquid helium, to a strand sample of about 100 mm length, up to 0.8% of the nominal bending strain at the surface of a wire with 0.8 mm diameter. The principal mechanism of the pure bending device is similar to that developed by W. Goldacker, et al. for characterization of high temperature superconductors under bending [4]. Our device was able to apply uniform bending to a strand under large electromagnetic forces, which were generated by the magnetic field and the transport current of the test sample. Details of the device have been described in [2] and [3].

Fig. 1 shows the variable bending sample holders and a gearbox to apply bending by accessing gears with a rotating shaft (not shown in the figure) from the top flange. Two sample holder plates are mounted on the beam clamps with lever arms. The sample holders are shown in **Fig. 2**. Grooved slots for the sample mounting are located at the top and bottom edges of each plate of the sample holder. The plate is made of Ti-6Al-4V with dimensions 1" x 6.5" x 0.063". In this way, the sample holder locates the neutral plane of the wire to apply pure bending to the samples. Two copper terminations are mounted at each end of the sample holder beam. The test wire is mounted on the beam before heat treatment, as shown in **Fig. 3,** along with witness samples of standard Jc sample holders. The grooves on the sample holder are fabricated with a 13 μm tolerance. It is known that the diameters of Nb_3Sn superconducting wires increase by a few percent after heat treatment. Therefore, the test wire should be tightly secured in the groove

during the experiment. Both ends of the test sample, 25 mm long, were soldered to the copper terminations on the beam after heat treatment. Each sample had a pair of voltage taps. The voltage tap separation was 50 mm and the distance between a voltage tap and the copper termination was 25 mm. **Fig. 4** shows a sample holder assembly of two beams mounted on beam clamps. A current lead was soldered to each copper termination. The sample holder beams were deformed to a true circular arc by rotational motions of the beam clamps to apply pure bending to the samples. The clamps were rotated by accessing gears with a rotating shaft from the top flange of the probe dewar. The shaft was driven by a ½ horsepower motor.
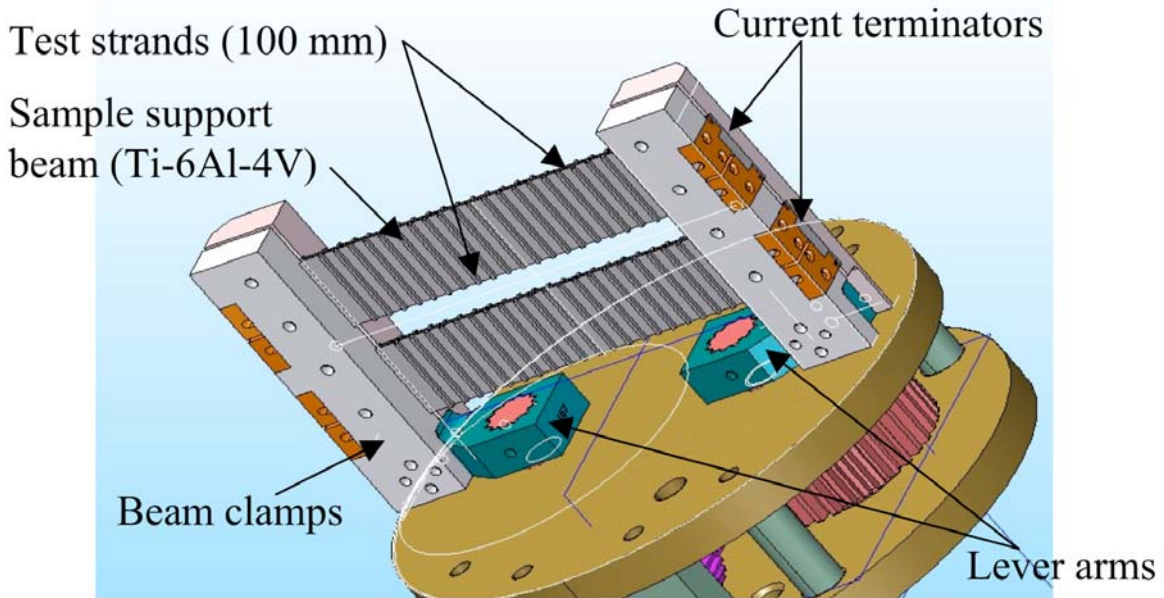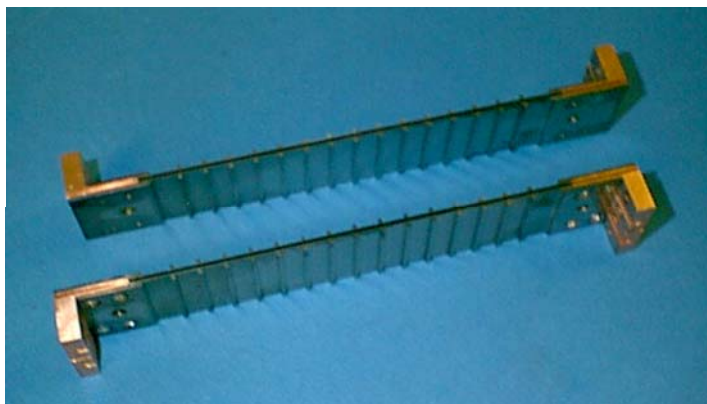

Fig. 1 Pure-bending device for four strand samples on two sample holder plates mounted on beam clamps rotated with a gear assembly.

(a)   (b)

Fig. 2 (a) Pure bending sample holders with copper terminations, which are enlarged in (b).
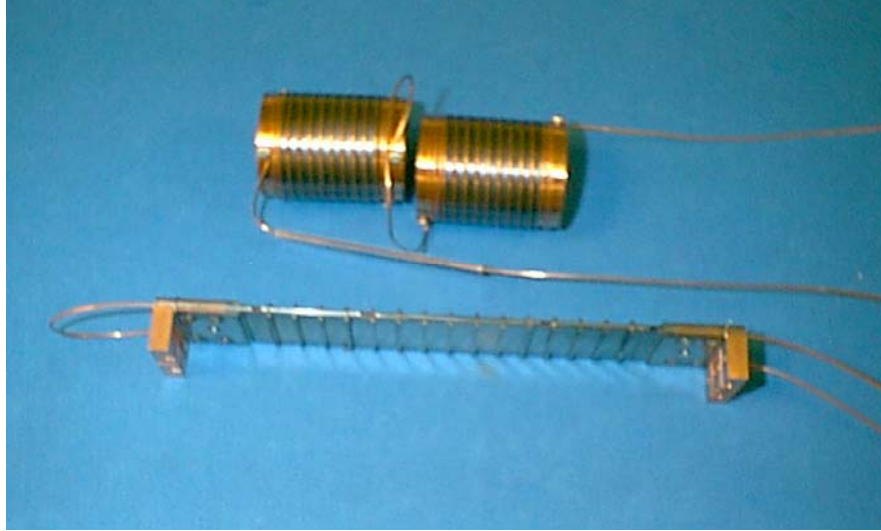
Fig. 3 Pure bending test samples mounted on the sample holder with witness Jc standard barrel samples before heat treatment.
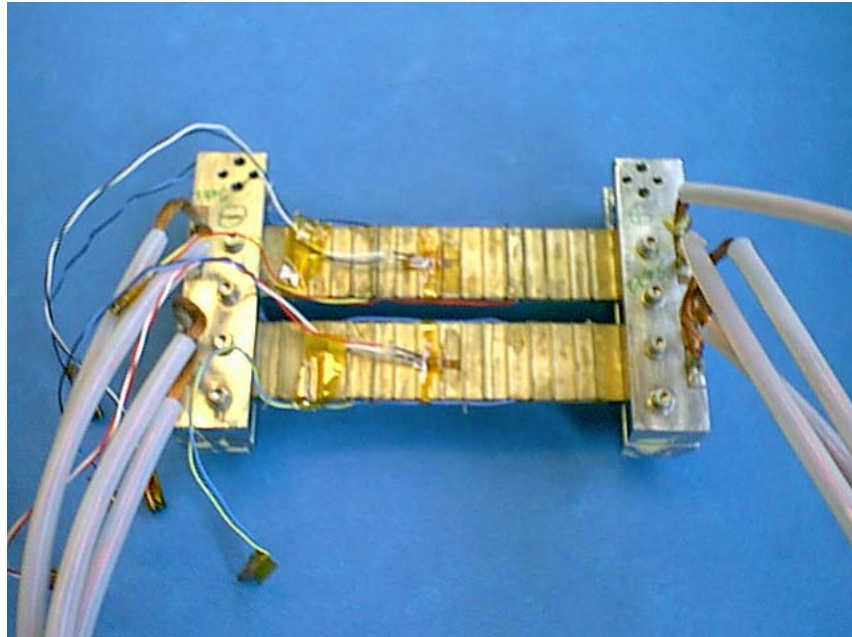

Fig. 4 Sample assembly of two beams of the pure bending sample holder on the beam clamps with current leads and strain gauges.

All tests were performed using the 20 T, 195 mm Bitter magnet at NHMFL, Florida State University. **Fig. 5** shows the experimental test set up with the data acquisition system, the magnet and the magnet cryostat with the pure bending test probe. The motor to drive the gears mounted on the test probe is shown with the cryostat and 500 L liquid helium dewar in **Fig. 6**.

Fig. 5 Pure bending test set up in the 20 T, 195 mm Bitter magnet cell at NHMFL.
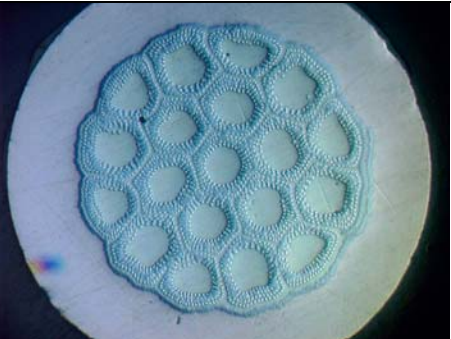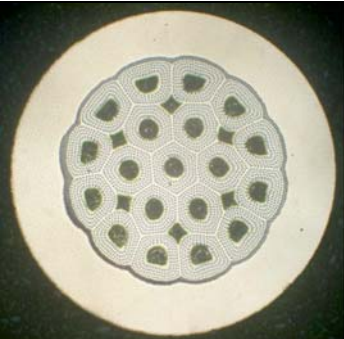

Fig. 6 The test probe with a gear driver motor is mounted from the top of the cryostat

We tested five different Nb_3Sn wires which were developed by the ITER parties. Three were internal-tin wires of recently developed ITER TF US Oxford and Luvata wires, and EU EM-LMI
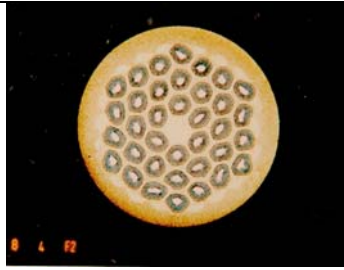
wire. Two of them were bronze wires of EU EAS and Japanese Furukawa designs, developed during the ITER Engineering Design Activity of the 1990's. Test wire characteristics and their heat-treatment schedules are shown in Tables I and II.

Table I ITER US TF Pre-production Oxford and Luvata wires.

Strand Manufacturer	Oxford	Luvata
Wire ID	B9355-2BE	NT8404
Technique	Internal tin	Internal tin
Strand Diameter (mm)*	0.817	0.818
Cu : non-Cu*	1.076	1.075
Twist pitch (mm)*	10	13
Heat treatment	Ramp up to 210 °C with 10 °C/h and hold for 50 hours, ramp up to 340 °C with 10 °C/h and hold for 25 hours, ramp up to 450 °C with 10 °C/h and hold for 25 hours, ramp up to 575 °C with 10 °C/h and hold for 100 hours, ramp up to 650 °C with 10 °C/h and hold for 200 hours.	Ramp up to 200°C with 10°C/h and hold for 50 hours, ramp up to 460°C with 15°C/h and hold for 50 hours, ramp up to 575°C with 50°C/h and hold for 100 hours, ramp up to 650°C with 50°C/h and hold for 175 hours, and Ramp down at 25°C/h.
Cross section		 Courtesy of Tae Pyon, Luvata.

* Manufacturer's data

Table II ITER related EU and Japanese wires. The EM-LMI and Furukawa wires are from the ITER model coil program.

Strand Manufacturer	EU EAS	EU EM-LMI	Japanese Furukawa
Wire ID	NSTT8305-HK002-A2	Wire used for BM3	SG-96071-08
Technique	Bronze	Internal tin	Bronze
Strand Diameter (mm)*	0.806	0.806	0.809
Cu : non-Cu*	0.92	1.38	1.58
Twist pitch (mm)*	15	9.9	17.9
Heat Treatment	Ramp up to 205 °C with 10 °C/h, ramp up to 210 °C with 5 °C/h and hold for 50 hours, ramp up to 340 °C with 10 °C/h and hold for 25 hours, ramp up to 450 °C with 10 °C/h and hold for 25 hours, ramp up to 575 °C with 10 °C/h and hold for 100 hours, ramp up to 660 °C with 10 °C/h and hold for 100 hours, and ramp down at 25 °C/h	Ramp up to 120°C with 20°C/h, ramp up to 180°C with 68°C/h, ramp up to 200°C with 20°C/h and hold for 50 hours, ramp up to 340°C with 68°C/h and hold for 24 hours, ramp up to 650°C with 68°C/h and hold for 200 hours, and ramp down at 73°C/h.	Ramp up to 650 °C with 50 °C/h and hold for 240 hours, and ramp down at 20 °C/h
Cross Section		Courtesy of A. Nijhuis, Univ. of Twente.	

* Manufacturer's data

The bending strain values mentioned above, for example 0.8%, are so called nominal values of the maximum bending strain at the wire surface. The actual peak bending strain of the filaments of the tested wires was about 67% of the nominal bending strain values. It means that 0.8% nominal bending is corresponding to about 0.54% peak filament bending. The ratio of the peak bending strain to the nominal bending strain, depends on the Cu:non-Cu ratio of the wire, scaling as the ratio of the strand diameter to that of the non-copper area.

The critical currents were measured at every 0.1% nominal bending up to 0.8%. Irreversible degradation of the critical current was measured by releasing bending after each 0.1% increment. The next sections show following test results of each wire:
1. The initial critical currents and n-values before applying bending as a function of the magnetic fields.
2. The critical currents measured in order of the test sequences.
3. The normalized critical currents as a function of the peak filament bending strains.

3. Test Results

3.1 ITER TF pre-production Oxford and Luvata wires

The initial critical current measured before applying bendings of Oxford and Luvata wires are shown with the n-values in **Fig. 7** (a) and (b), respectively. **Fig. 8** shows the critical currents at 12 T to 15 T before and after the 0.8% nominal bending.
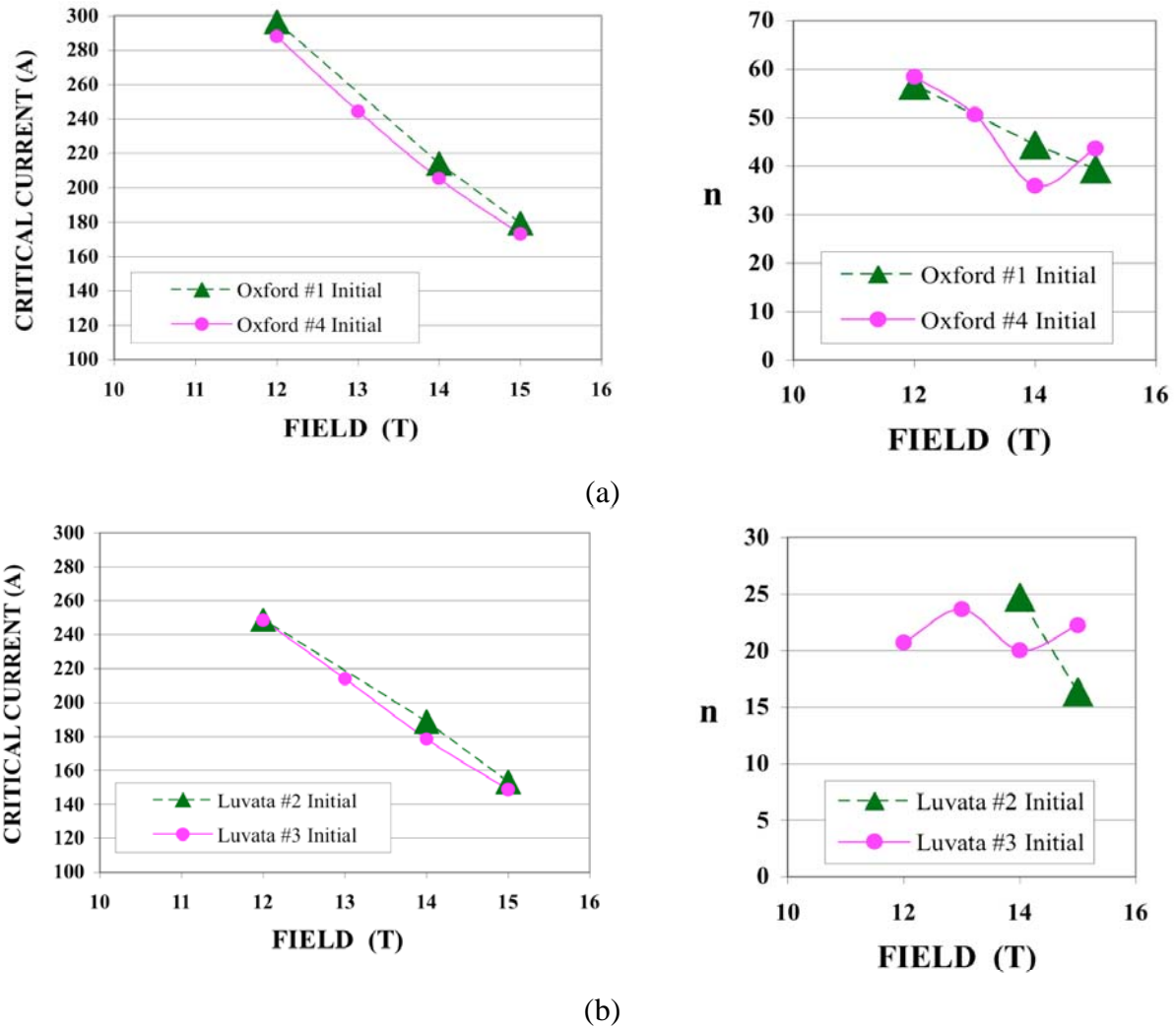

(a)

(b)

Fig. 7 Initial critical currents and n-values of Oxford and Luvata wire samples measured before applied bending strains. (a) Oxford wire, and (b) Luvata wire.
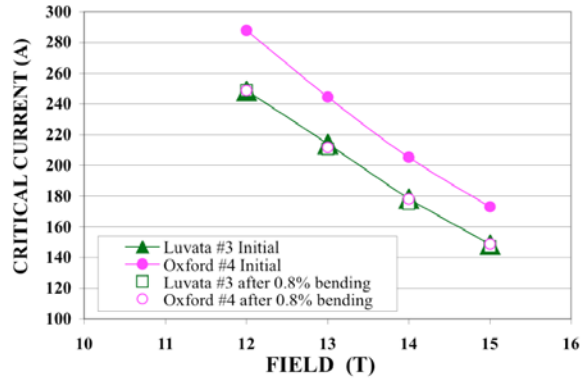
Fig. 8 The critical currents Oxford and Luvata wires at 15 T before and after applying 0.8% nominal bending. Oxford wire shows a significant degradation after the bending.

The following figures show pure-bending test results of Oxford and Luvata wires at 15 T. The normalized critical currents are plotted for the nominal bending strains in test sequence. **Fig. 9** is for two samples of Oxford wire, and **Fig. 10** is for two samples of Luvata wire.
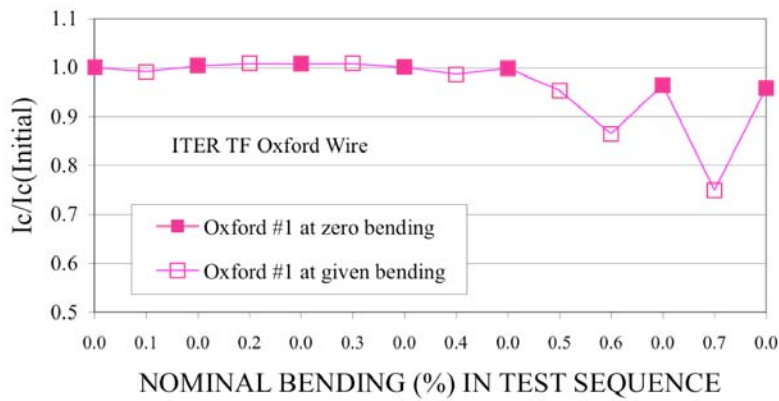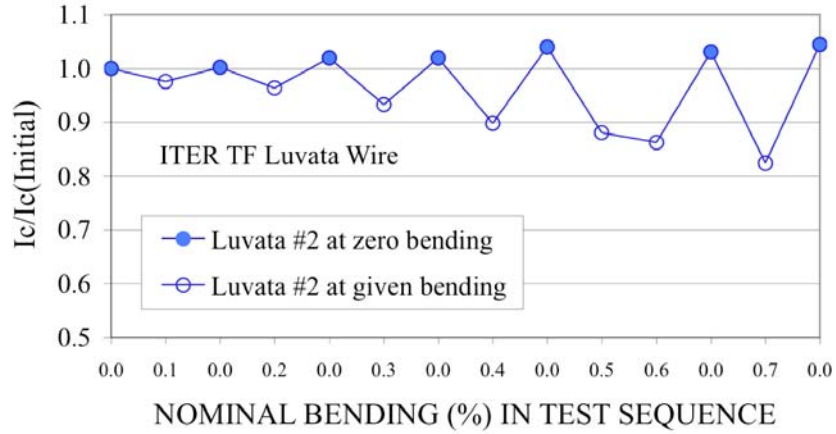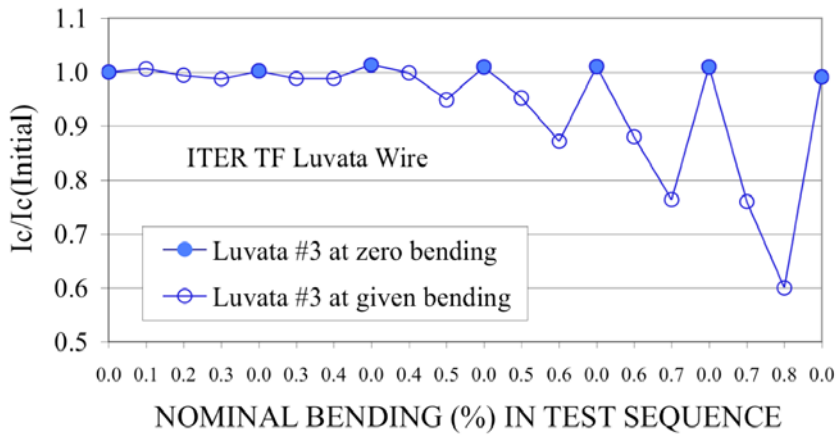

(a)
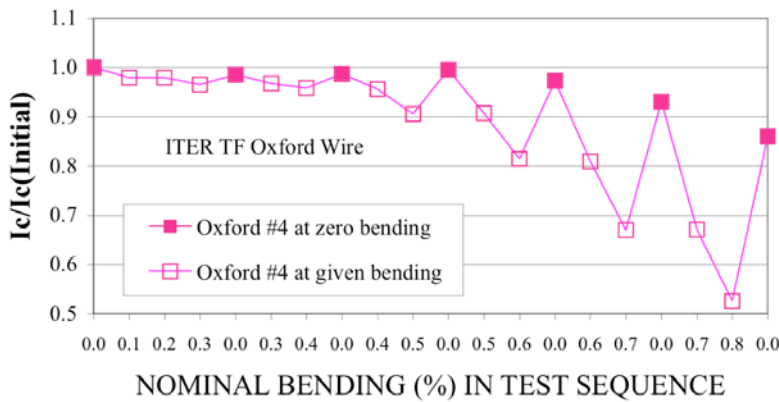
(b)

Fig. 9 The normalized critical currents of two Oxford wire samples are plotted for the nominal bending strains in the order of testing. (a) Luvata strand, (b) Oxford strand.

(a)

(b)

Fig. 10 The normalized critical currents of two Luvata wire samples are plotted for the nominal bending strains in test sequence.

In **Figs. 11** and **12**, the bending test results of Oxford and Luvata wires are plotted as a function of the peak filament bending strains, respectively. As seen in these figures the critical currents degraded with increasing bending strains. At about 0.55% peak filament bending strains the critical currents were degraded by 47% for Oxford wire and 40% for Luvata wire. The initial critical currents of the Luvata and Oxford wires were very similar to each other. However, the irreversible degradations of Oxford and Luvata wires after the 0.8% nominal bending were about 13% and 1.3%, respectively. It is noted that there is a significant difference of the bending effect between those two wires, even though both wires were made by internal tin Nb_3Sn process to identical specifications.
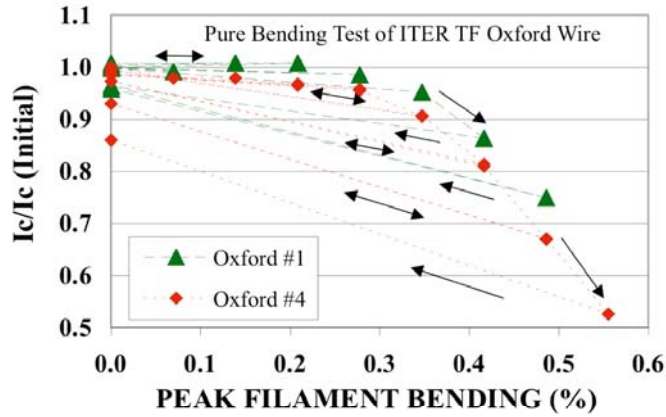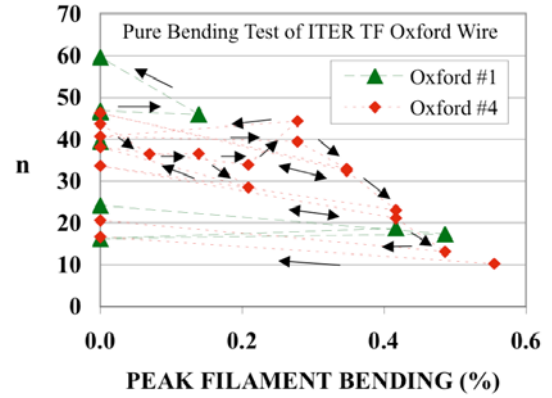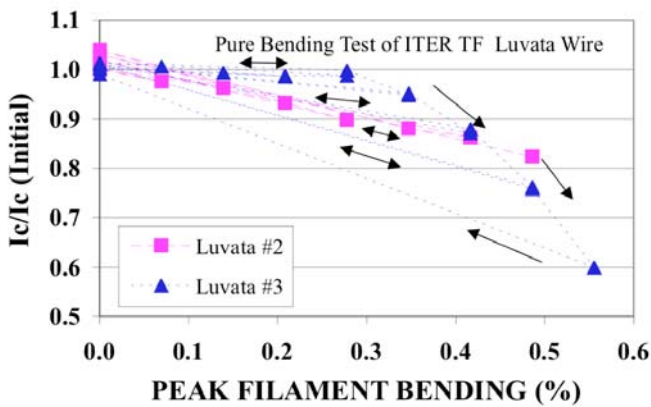
(a)   (b)
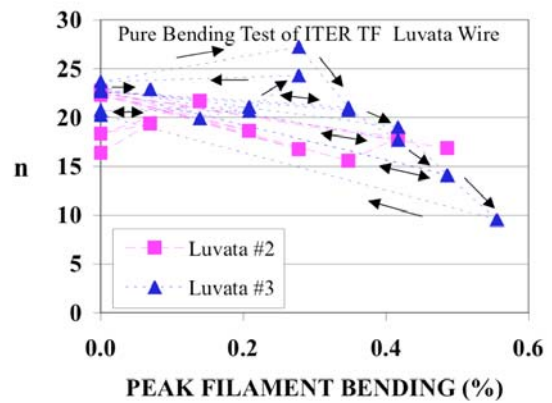
Fig. 11 Normalized critical currents and n-values as a function of the peak filament bending strains for Oxford wire.

(a)   (b)

Fig. 12 Normalized critical currents as a function of the peak filament bending strains for Luvata wire.

A typical motor speed for ramping up and down used for the bending test was about 0.0015% of the nominal bending rate per second for a 0.8 mm diameter wire. A motor of ½ horsepower was selected to obtain much faster speeds in order to perform a cyclic bending test. At the end of the series bending tests, a quick ramp test was performed in liquid helium. When the ramping speed was increased to 0.0046% per second, which was three times faster than the normal test speed, one of the sample holder beams was broken just before reaching 0.8% bending, as shown in **Fig. 13**.
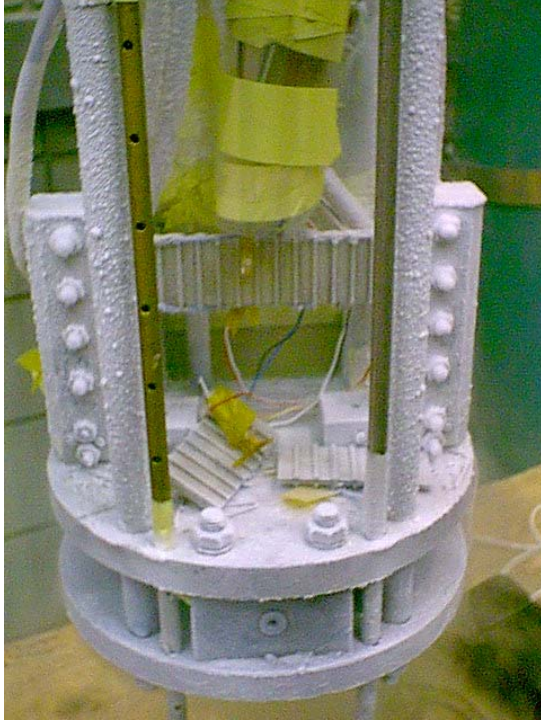
(a)
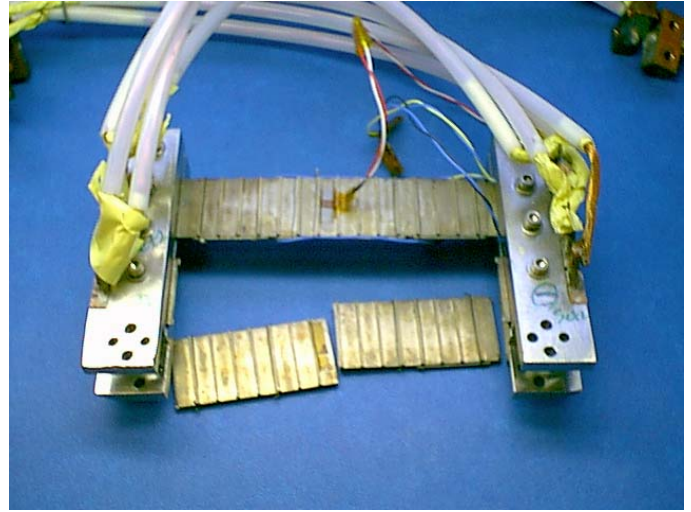
(b)

Fig 13 One of the pure bending beams was broken just before reaching 0.8% bending when the bending was applied at the fast rate of 0.0046% per second, which was three times faster than the normal speed.

3.2 Other ITER-related wires

In the second series of bending tests, three wires were tested. One of them was an EAS advanced bronze wire developed recently by the EU, and the others were EM-LMI internal-tin and Japanese Furukawa bronze wires, both developed for the ITER Model Coil program. These wires were tested in the same way as that used for the Oxford and Luvata wires, but the magnetic field strength for the bending tests of these samples was 12 T instead of 15 T, since there was a magnet problem for 15 T operation. Test results for each wire are shown below.

3.2.1 EU EAS Wire

Fig. 14 shows the critical currents and n-values of an EAS wire sample measured at 12 T to 15 T before bending. The normalized critical currents measured with various bending at 12 T are plotted with the nominal bending strains in test sequence in **Fig. 15**, and also are plotted as a function of the peak strain with n-values in **Fig. 16**. The critical current of the EAS sample degraded by 12 % at 0.58% peak filament bending (0.8% nominal bending). Permanent degradation was about 2%.

(a)   (b)

Fig. 14 Initial critical currents and n-values of EAS wire sample measured before applied bending strains.

Fig. 15 The normalized critical currents of two EAS wire samples are plotted for the nominal bending strains in the order of testing

(a)   (b)

Fig. 16 Normalized critical currents and n-values as a function of the peak filament bending strains for the EAS wire sample.

15

3.2.2 EM-LMI Wire (ITER model coil wire)

The critical currents and n-values of three EM-LMI samples measured between 12 T and 15 T before bending are shown in **Fig. 17**. The normalized critical currents of these three samples measured at 12 T are plotted with the nominal bending strains in the test order in **Figs. 18, 19** and **20**. **Fig. 21** plots the critical currents and n-values as a function of the peak filament bending strain. A four-cycle test at the nominal 0.8% bending (0.52% peak bending) was performed for the EM-LMI #3 sample, as shown in **Fig. 20**. After four-cycle operation between 0% and 0.52% peak bending, the critical current was slightly decreased from 80% to 77% at the peak bending 0.52%. Overall the critical current of EM-LMI samples degraded by about 30% at the 0.52% peak bending. However, it was noticed for the EM-LMI samples that the critical currents at the zero bending strain seemed to increase very gradually after each bending strain cycle.

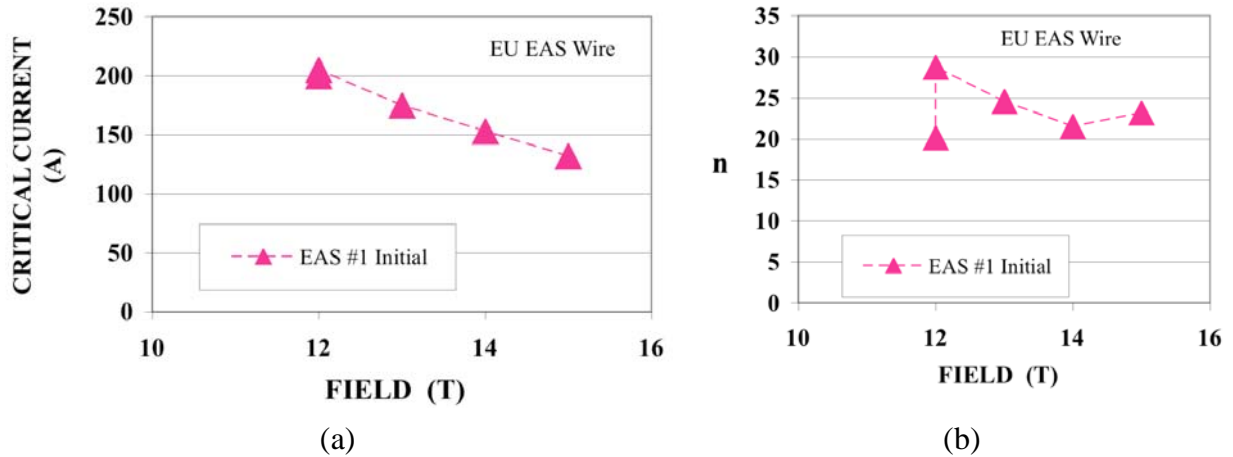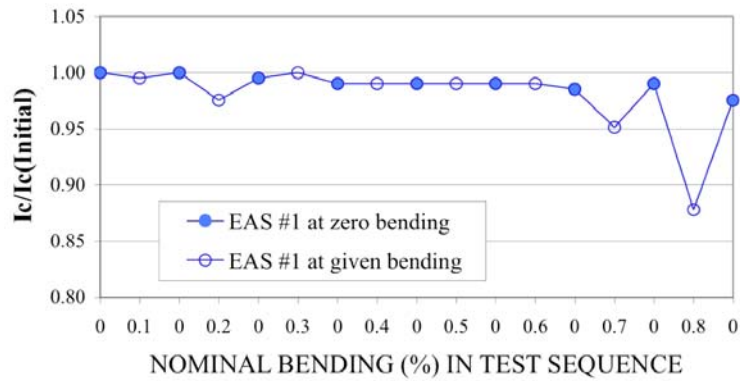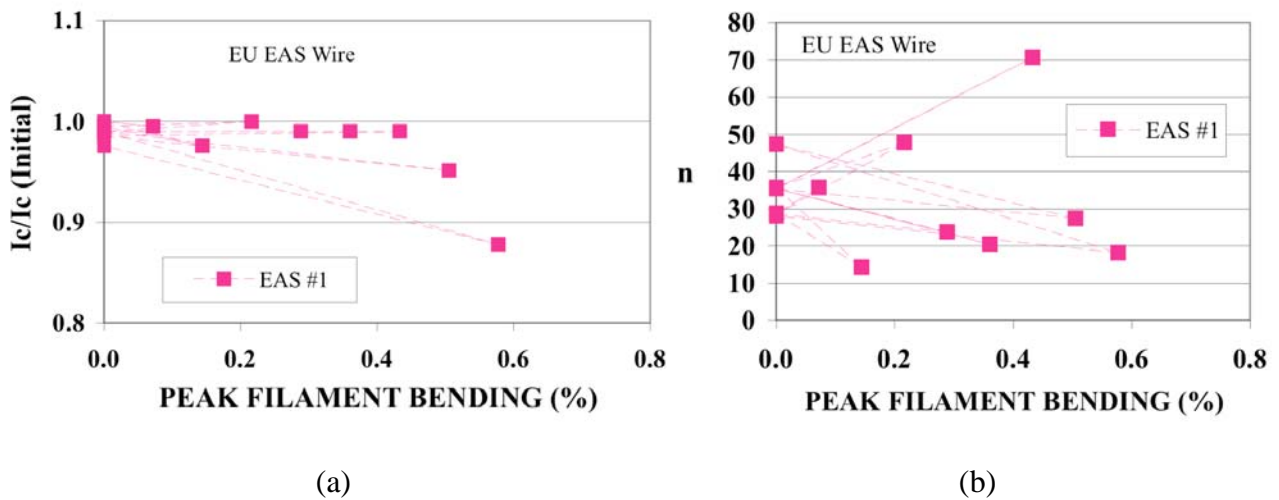(a)   (b)

Fig. 17 Initial critical currents and n-values of three EM-LMI wire samples measured before applied bending strains.

Fig. 18 The normalized critical currents of EM-LMI wire sample #1 are plotted for the nominal bending strains in the order of testing.

Fig. 19 The normalized critical currents of EM-LMI wire sample #2 are plotted for the nominal bending strains in the order of testing.

Fig. 20 The normalized critical currents of EM-LMI wire sample #3 are plotted for the nominal bending strains in the order of testing.

(a)   (b)

Fig. 21 Normalized critical currents and n-values of three EM-LMI samples as a function of the peak filament bending strains.

17

3.2.3 Furukawa Wire (ITER model coil wire)

The critical currents and n-values measured before bending for three Furukawa samples are shown in **Fig. 22**. The normalized critical currents of these three samples measured at 12 T are plotted with the nominal bending strains in the order of testing in **Figs. 23, 24** and **25**. **Fig. 26** plots the critical currents and n-values as a function of the peak filament bending strain. A four-cycle test of the nominal 0.8% bending (0.50% peak bending) was performed for two Furukawa samples (#3 and #4). Critical current changes due to the cyclic test were negligible. The critical currents of the Furukawa samples degraded by 12% at the 0.50% peak bending. As seen for the EM-LMI samples in **Figs. 19** and **20**, the critical currents of the Furukawa samples at the zero bending strain increased gradually after each bending cycle, and also it was noticed for Furukawa samples that the critical currents increased by 1% at the peak bending strains of about 0.3%.

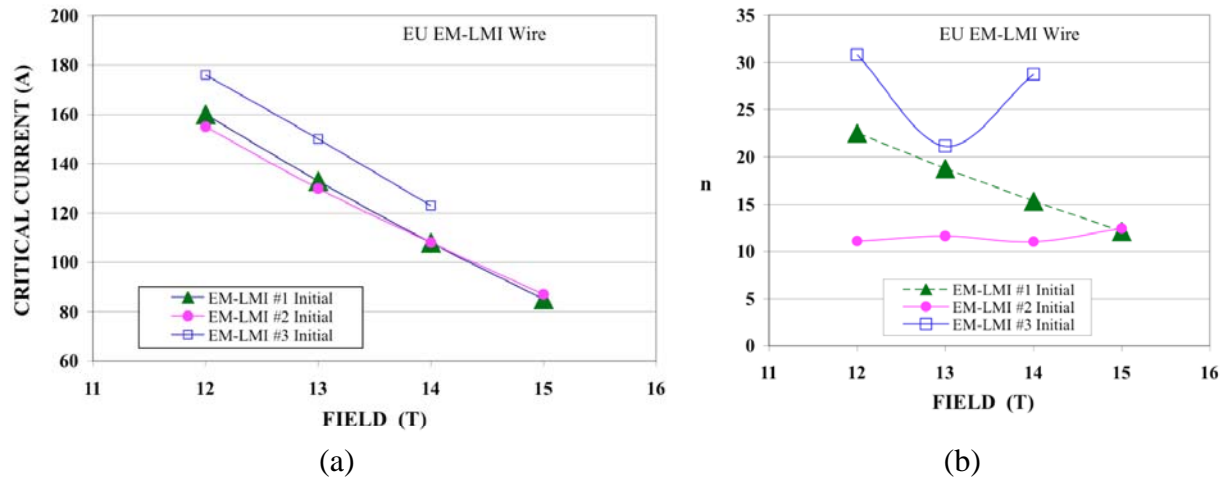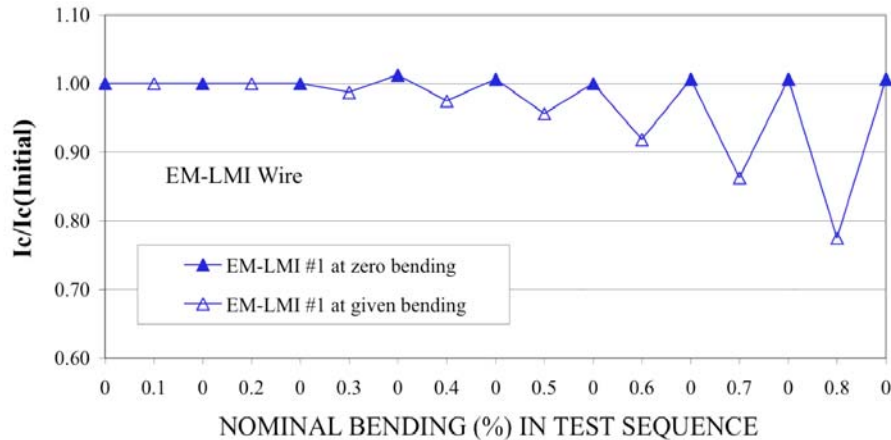(a)   (b)
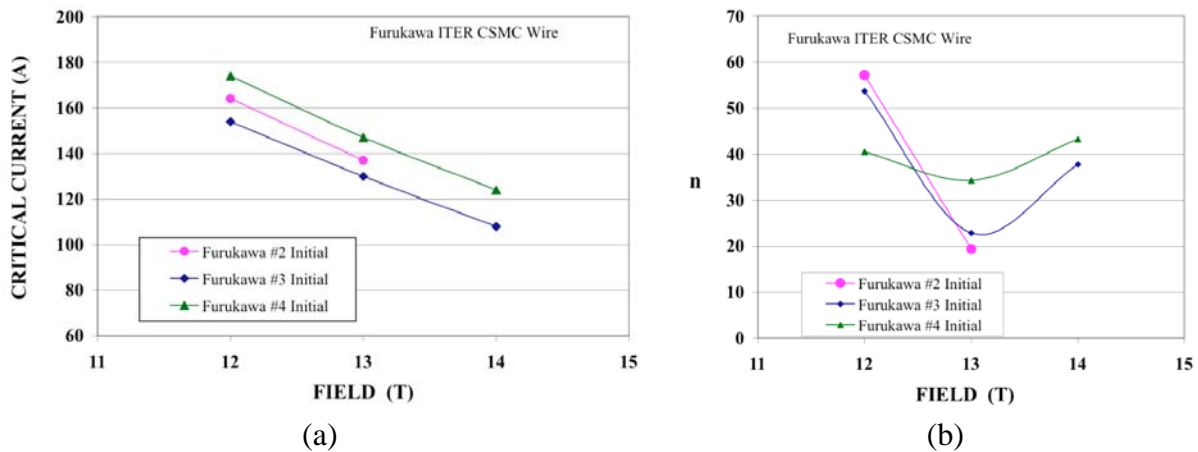
Fig. 22 Initial critical currents and n-values of three Furukawa wire samples measured before applying bending strains.
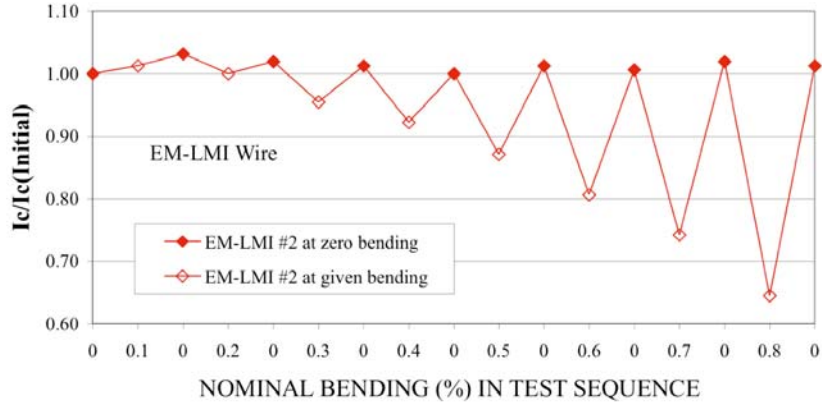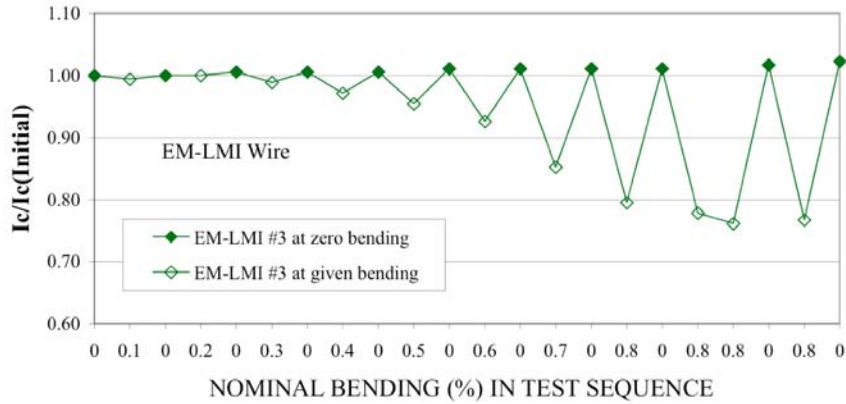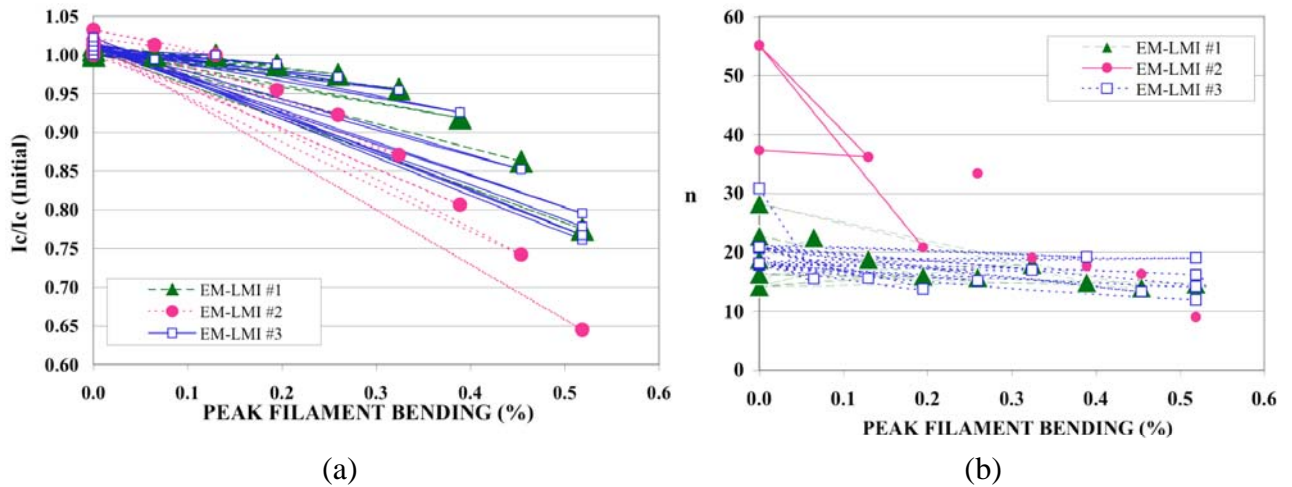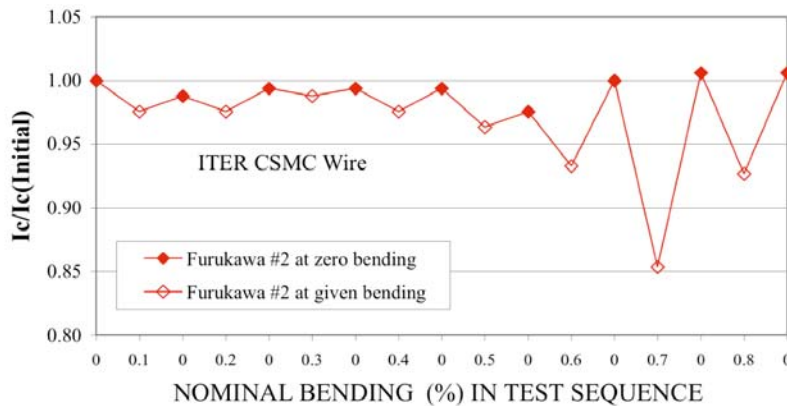

Fig. 23 The normalized critical currents of Furukawa wire sample #2 are plotted for the nominal bending strains in the order of testing
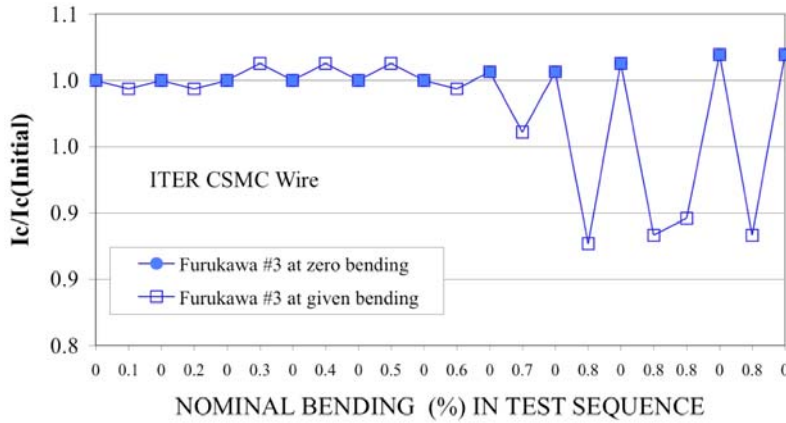
Fig. 24 The normalized critical currents of Furukawa wire sample #3 are plotted for the nominal bending strains in the order of testing
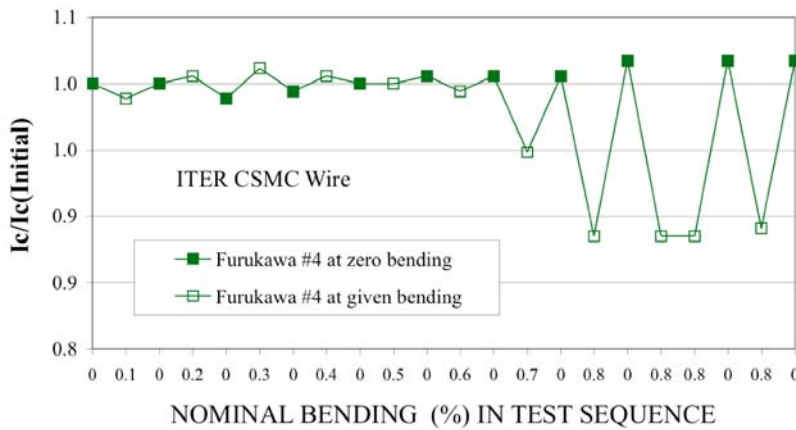
Fig. 25 The normalized critical currents of Furukawa wire sample #4 are plotted for the nominal bending strains in the order of testing

| (a) | (b) |
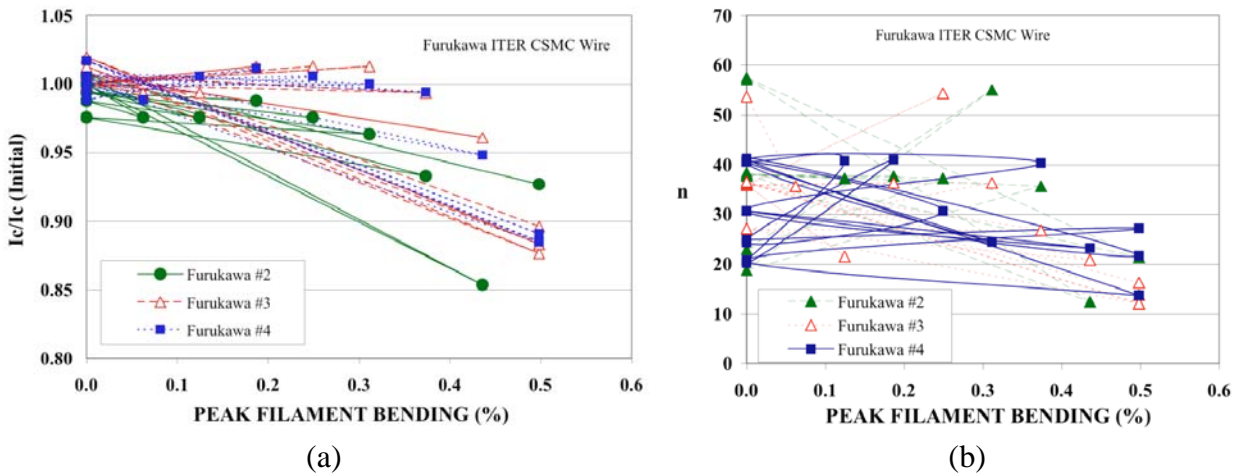
Fig. 26 Normalized critical currents and n-values as a function of the peak filament bending strains for Furukawa wire samples.

19

4. Model Analysis

4.1 Critical Current Formula

To analyze the critical current of the bending effects, the scaling formula recommended recently by Bottura [5], which was distributed by Arnaud Devred as part of an ITER official acceptance criterion, was used. The critical current density is given:

$$J_c = \frac{C}{B} s(e)(1 - t^{1.52})(1 - t^2)b^p (1 - b)^q \tag{1}$$

The strain function:

$$s(\varepsilon) = 1 + \frac{1}{1 - C_{a1}\varepsilon_{0a}}\left[C_{a1}(\sqrt{\varepsilon_{sh}^2 + \varepsilon_{0a}^2} - \sqrt{(\varepsilon - \varepsilon_{sh})^2 + \varepsilon_{0a}^2}) - C_{a2}\varepsilon\right] \tag{2}$$

(2)

$$\varepsilon_{sh} = \frac{C_{a2}\varepsilon_{0,a}}{\sqrt{C_{a1}^2 - C_{a2}^2}} \tag{3}$$

Reduced magnetic field: $\quad b = \dfrac{B}{B_{C2}^*(T, \varepsilon)}$ \hfill (4)

Reduced magnetic field at zero temperature: $\quad b_0 = \dfrac{B}{B_{C2}^*(0, \varepsilon)}$ \hfill (5)

Reduced temperature: $\quad t = \dfrac{T}{T_C^*(0, \varepsilon)}$ \hfill (6)

Critical temperature: $\quad T_C^*(B, \varepsilon) = T_{C0\,max}^*[s(\varepsilon)]^{\frac{1}{3}}(1 - b_0)^{\frac{1}{1.52}}$ \hfill (7)

Critical field: $\quad B_{C2}^*(T, \varepsilon) = B_{C20\,max}^* s(\varepsilon)(1 - t^{1.52})$ \hfill (8)

C = The scaling constant
$B_{C20\,max}^*$ = The upper critical field at zero temperature and strain
$T_{C0\,max}^*$ = The critical temperature at zero field and strain
p = The low field exponent of the pinning force ($p < 1$, $p \approx 0.5$)
q = The high field exponent of the pinning force ($q \approx 2$)
C_{a1} = The strain fitting constant
C_{a2} = The strain fitting constant
ε_{0a} = The residual strain component
ε_{max} = The tensile strain at which the maximum critical properties are reached.

4.2 Conventional Model of Bending Effects on Strand Critical Current

The critical current of a multi-filamentary superconducting strand under bending strain has been formulated by Ekin [6], and his concept has been adopted for various work [7]-[10]. Ekin considered critical current distributions due to uniaxial strain geometry in twisted filaments of a strand under bending while taking into account the current transfer length between filaments with regards to the twist pitch length. Two extreme cases have been considered; long twist pitch (or low inter-filament resistivity), and short twist pitch (or high inter-filament resistivity). We will call the former case "Perfect Current Transfer," and the latter "No Current Transfer."

Perfect current transfer

If currents can transfer between filaments without electric loss (zero transverse resistance), the critical current of a multifilamentary strand can be obtained from the total current of one cross-section of a strand [6]. The critical current of a strand is given by

$$I_c = 2\int_{-R_{nc}}^{R_{nc}} j_c(\varepsilon_y)\sqrt{R_{nc}^2 - y^2}\,dy \qquad (9)$$

here,
R_{nc}=The radius of the non-copper area

$$\varepsilon_y = \varepsilon_0 + \varepsilon_{by} \qquad (10)$$
ε_0 =The precompressive strain
$$\varepsilon_{by} = \frac{y}{R_b} \qquad (11)$$

No current transfer

If the transverse resistance between filaments is high enough and no current can transfer between filaments, the critical current of each filament can be limited by the worst point in one twist pitch with regard to bending strain distributions. Therefore the current of a strand is given by [6]

$$I_c = 2\pi \int_0^{R_{nc}} j_c(\varepsilon_y)y\,dy \qquad (12)$$

here,

$$\varepsilon_y = \varepsilon_0 + \varepsilon_{by} \qquad (10')$$

$$\varepsilon_{by} = \begin{cases} -\dfrac{y}{R_b} & for\ j_c(\varepsilon_0 - \dfrac{y}{R_b}) < j_c(\varepsilon_y + \dfrac{y}{R_b}) \\[2mm] +\dfrac{y}{R_b} & for\ j_c(\varepsilon_0 - \dfrac{y}{R_b}) > j_c(\varepsilon_y + \dfrac{y}{R_b}) \end{cases} \qquad (13)$$

Note that the worst point of the critical current does not occur always at the compression side. At a large bending rate the tension side may happen to create larger degradation of the critical

current than the compression side since the critical current decreases at the tension side more sharply than at the compression side. Eq. (14) takes care of this effect. We introduce an minimum function operator to express a minimum value of $j_c(\varepsilon)$ in the range of strains between $-\varepsilon_{by}$ and $+\varepsilon_{by}$. Using the minimum function operator, Eqs. (12)-(13) can be written as,

$$I_c = 2\pi \int_0^{R_{nc}} \left\{ \min\left| j_c(\varepsilon_y) \right|_{\varepsilon_y = \varepsilon_0 - \varepsilon_{by}}^{\varepsilon_y = \varepsilon_0 + \varepsilon_{by}} \right\} y \, dy \tag{14}$$

where,

$$\varepsilon_{by} = \frac{y}{R_b} \tag{11'}$$

4.3 Integrated Model

In general it has been known that the experimental results of the critical currents under a wide range of bending strains fit neither the Perfect Current Transfer model nor the No Current Transfer model. Our experimental results were only a good fit to the Perfect Current Transfer model at small bending rates, and then sharply drop off toward the prediction line of No Current Transfer model with increasing bending. We have investigated various effects due to mechanical bending, that is, neutral-axis shift [6], [11], [12], current transfer length, filament breakage [13], and uniaxial strain releasing [11], [14].

Neutral-Axis Shift Effect

A shift of the neutral-axis due to yielding of the strand matrix under bending has been pointed out by Ekin [6]. When the neutral-axis shifts toward the compressive side by δ as shown in Fig. 27. The bending strain ε_{by} is given by

$$\varepsilon_{by} = \frac{y + \delta}{R_b - \delta} \tag{15}$$

The peak bending strain on the tension and compression sides are written respectively as,

$$\varepsilon_{bp}^+ = \frac{R_{nc} + \delta}{R_b - \delta} \tag{16}$$

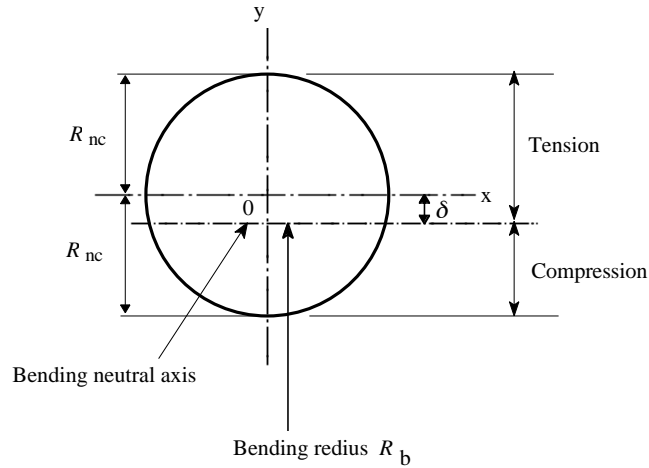$$\varepsilon_{bp}^- = -\frac{R_{nc} - \delta}{R_b - \delta} \tag{17}$$

22

Fig. 27 Cross-section of non-copper showing the neutral axis shift of δ.

The critical current for Perfect Current Transfer and No Current Transfer can be obtained using Eqs. (15)–(17) by Eq. (9) and Eq. (14), respectively. All integrations in this work were carried out by the Gaussian integration method of order 40 using Microsoft Excel®.

Figs. 28 and 29 show the calculated neutral-axis shift effect on the critical current for the Perfect Current Transfer and No Current Transfer cases, respectively. As seen here, there are significant differences between the Perfect Current Transfer and No Current Transfer cases. In the Perfect Current Transfer case the critical current shows a maximum peak at certain conditions of bending and neutral axis shift since the tension area increases. This was observed for the Furukawa wire (Fig. 26). However, in the No Current Transfer case there is no such peak, since the critical current is dominated by the worst point of the critical current.
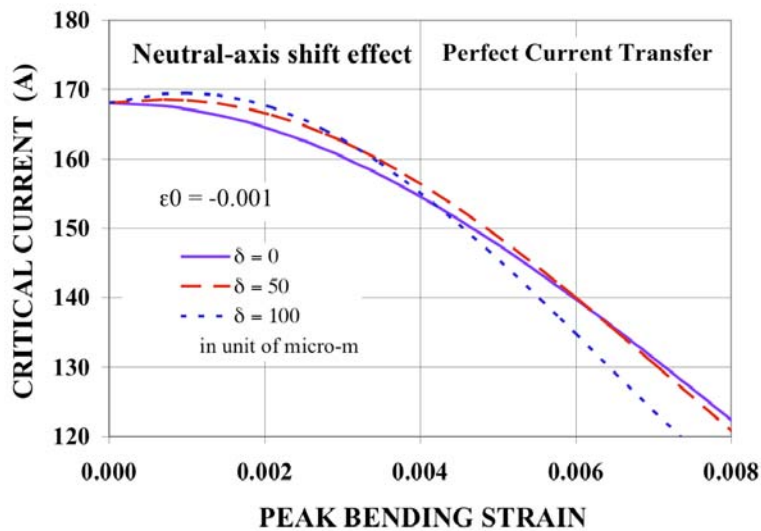

Fig. 28 Calculated critical currents of neutral-axis shift effect for Perfect Current Transfer.
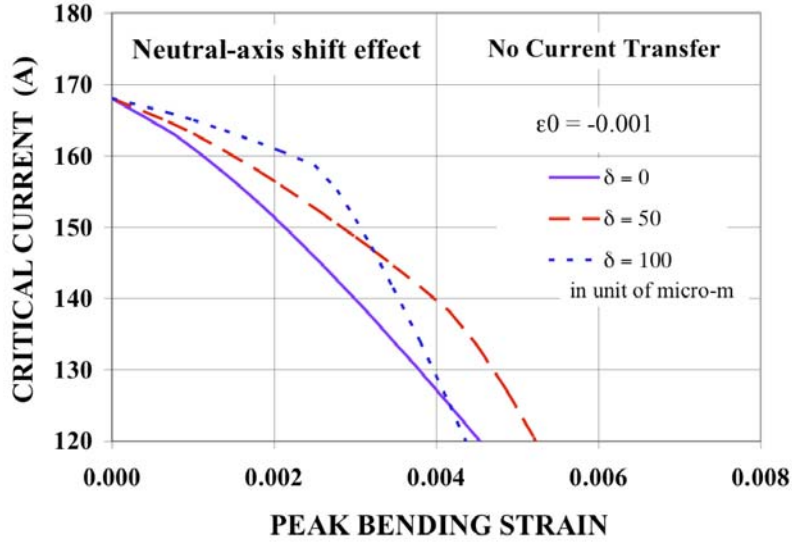
Fig. 29 Calculated critical currents of neutral-axis shift effect for No Current Transfer.

Current Transfer Length Effect

As mentioned earlier, all trends of measured critical currents at various bending strains are between those of Perfect Current Transfer and No Current Transfer. The current transfer length affects the total critical currents with regard to the twist pitch length L_p since the critical current changes periodically along a filament. Therefore the ratio of the current transfer length and the twist pitch, L_{ct}/L_p, will be an important factor for critical current behavior. The current transfer length L_{ct} has been give as a function of the transverse resistance of matrix material between filaments and the n-value of the resistive transition of the superconductor by [15], [16], [9],

$$L_{ct} = d \sqrt{\frac{0.106}{n} \frac{\rho_m}{\rho^*}} \tag{18}$$

here,
n = The empirical power factor ($\rho = kJ^n$) representing the resistive transition in the superconductor
ρ_m = The transverse resistance of the matrix between filaments
ρ^* = The superconductor resistivity criterion of the critical current
d = The conductor diameter[15]. Ref. 9 used the strand diameter for d, however the diameter d is a measure with regard to the current transfer spacing between filaments, therefore d could be much smaller than the strand diameter.

It is noted that regardless of the accuracy of the current transfer length itself, the relative ratio of the current transfer length to the twist pitch (L_{ct}/L_p) is an important factor for characterizing the current transfer effects on the critical current. It should be emphasized that the current transfer length is a function of the n-value, as well as the transverse resistance.

To take into account the current transfer effect, the critical current of a filament at a given point z along a filament is assumed to be dominated by the minimum critical-current value between z - $L_{ct}/2$ and z + $L_{ct}/2$. Now the critical current can be given using the minimum function operator defined for Eq. (14) as in cylindrical coordinates,

$$I_c = 2\int_0^{R_{nc}} \int_{-\frac{\pi}{2}}^{\frac{\pi}{2}} \left\{ \min \left| j_c(\varepsilon_{r\phi}) \right|_{\phi=\varphi-\varphi_{ct}}^{\phi=\varphi+\varphi_{ct}} \right\} r\, d\varphi\, dr \tag{19}$$

where,

$$\varepsilon_{r\phi} = \varepsilon_0 + \varepsilon_{br\phi} \tag{20}$$

$$\varepsilon_{br\phi} = \frac{r \sin\phi}{R_b} \tag{21}$$

$$\varphi_{ct} = \frac{2\pi L_{ct} \sin\theta}{L_p} \tag{22}$$

$$\theta = \tan^{-1} \frac{L_p}{2\pi R_{nc}} \tag{23}$$

L_{ct} =The minimum current transfer length
L_p =The twist pitch length of strand

Fig. 30 shows the calculated critical currents as functions of current transfer length effects with various current transfer lengths L_{ct} of 0.5 mm, 1 mm, 2.5 mm and 5 mm for a strand with the twist pitch L_p = 10 mm. These L_{ct} values correspond to 0, 5%, 10%, 25% and 50% of the twist pitch length. The curves of L_{ct} = 0 and L_{ct} = 0.5 L_p agree with the results of Perfect Current transfer (red open circle) and No Current transfer (Blue open triangle), respectively.

To apply the neutral-axis shift effect to the current transfer model, the strain Eq. (21) is replaced to the following equation,

$$\varepsilon_{br\phi} = \frac{r \sin\phi + \delta}{R_b - \delta} \tag{24}$$
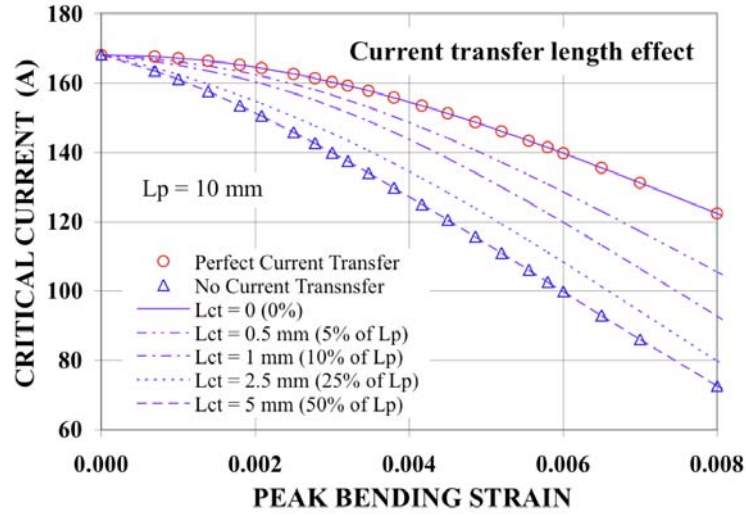
Fig. 30 Calculated critical currents of current transfer effect with various current transfer length L_{ct}.

Filament Breakage Effect

Filament breakages in the tension side due to bending have been found [13]. Such filament breakage is probably the dominant cause of the irreversible permanent degradation. If the filament breakage occurs on the surface of the tension side as shown in Fig. 31, the critical currents can be obtained with integration over the unbroken area in the above-mentioned methods. Note that in the case of No Current Transfer the effective superconducting filaments are only in the center circular section which does not overlap the broken area, since the strand is twisted. Therefore degradations of the No Current Transfer case due to breakage are much more significant than those of the Perfect Current transfer case.
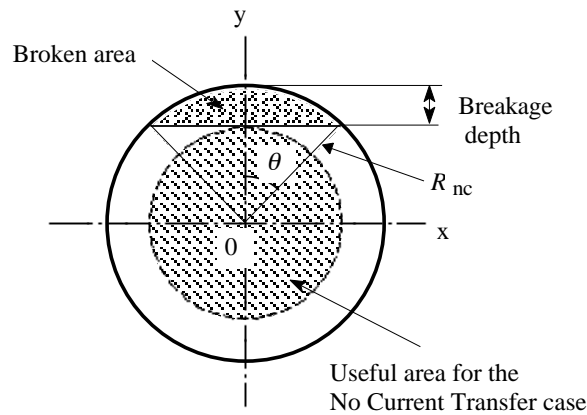

Fig. 31 Schematic of non-copper area having broken filament area.

Fig. 32 shows the calculated critical currents of the filament breakage for the Perfect Current Transfer (dark color lines) and No Current Transfer (light color lines) cases with the breakage

26

fractions of 0%, 2% and 5%. In the case of Perfect Current Transfer, critical current degradations are the same rates of the breakages. On the other hand the degradations of the No Current Transfer case are significant, for example about 35% for the 5% breakage at zero bending, since the outer layer filaments in the annulus of the breakage depth pass the broken area in one twist pitch as illustrated in Fig. 31. The filament breakage effects of those cases on the critical currents are shown as a function of the breakage in Fig. 33. The relationship between the breakage fraction and the breakage depth is shown in Fig. 34. The 5% breakage corresponds to the breakage depth of about 55 μm for the non-copper area diameter of 567 μm (10% of the non-copper diameter).

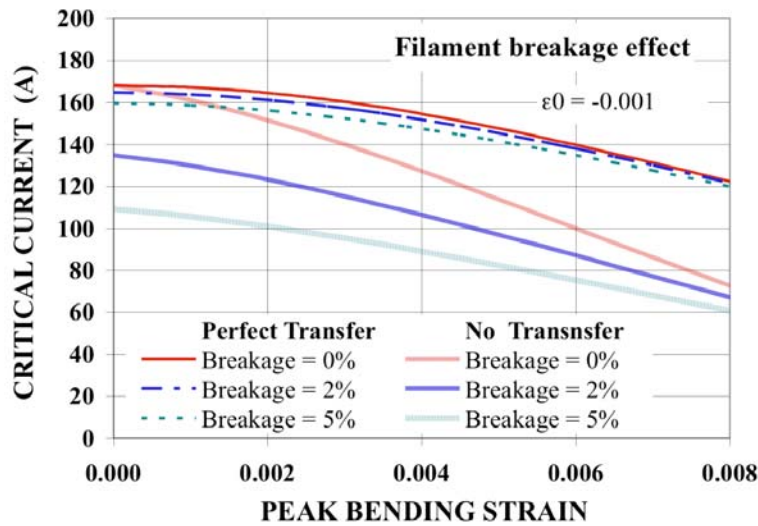Fig. 32 Calculated critical currents of the filament breakage effect of the Perfect Current Transfer (dark color lines) and No Current Transfer (light color lines) cases for the breakage fractions of 0%, 2% and 5%.
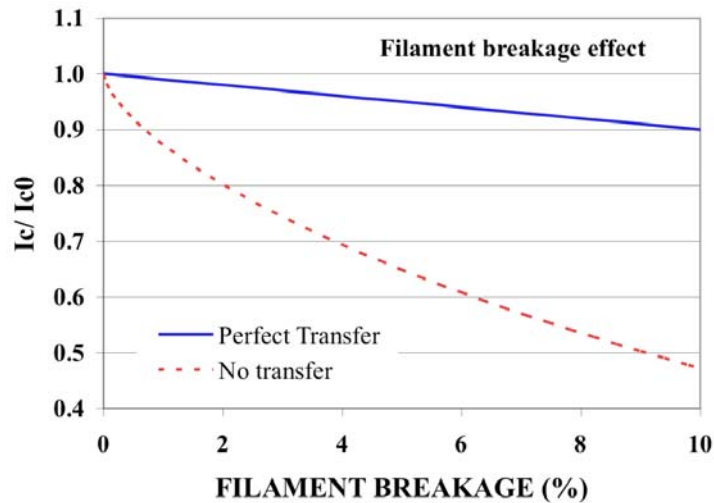

Fig. 33 Filament breakage effects on the critical currents for Perfect Current Transfer (dark color lines) and No Current Transfer (light color lines) as a function of the breakage.
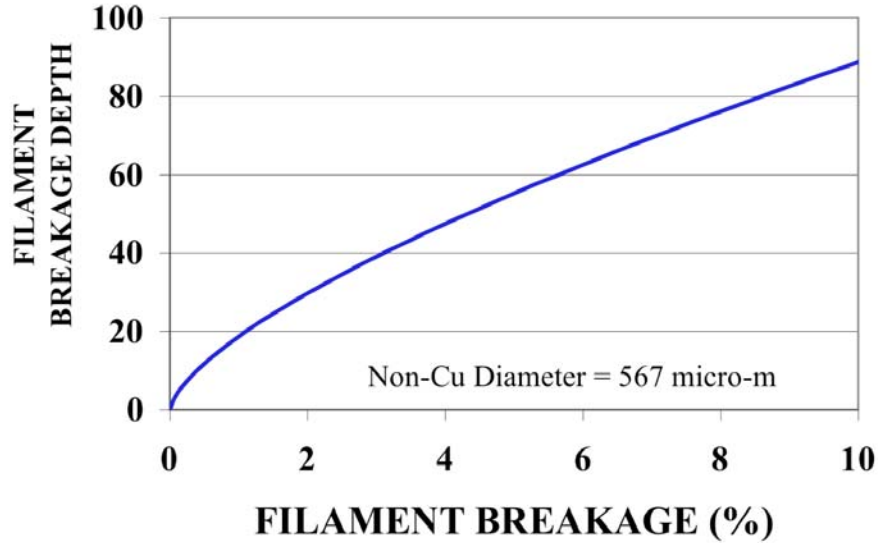
Fig. 34 Breakage depth as a function of the breakage fraction.

Uniaxial Strain Releasing Effect

Uniaxial thermally induced precompressive strain during cooldown after reaction of a Nb_3Sn wire could be released by mechanical bending cycles [14]. The result is that the strain $|\varepsilon_{max}|$ becomes smaller and the critical current increases. The increase of the critical current at zero bending after bending cycles could be driven only by this strain releasing effect. In the present experiments this effect seemed to be very small, but to happen for some wires.

5. Discussion

Five different Nb_3Sn wires were tested. The critical current of each wire is different under bending strains. The neutral axis shift explains the increase of the critical currents at small bending strain before large degradations. The current transfer length expresses deviations of experimental results from Perfect and No Current Transfer Models. The filament breakage shows the irreversible permanent degradation after mechanical cycles of bending strains. The uniaxial strain release could explain the slight increase of the critical currents after bending cycles.

To use the scaling law of Eq. (1) for analyses of the experimental results, parameters required for the equation were selected on the bases of various published work [5], [17]-[19]. There was no parameter study of the scaling law for the exact wires used here. Therefore a few parameters were adjusted by our measured critical current results of magnetic field dependences. The parameters used for the tested wires are summarized in Table III. The parameters of p and q were p=0.5 and q=2.

Table III Scaling equation parameters used for curve fittings.

Strand	Oxford	Luvata	EAS	EM-LMI	Furukawa
B^*_{c20max} (T)	32.5	32.5	35.75	28.7	32.5
T^*_{c0max} (K)	17.8	17.0	16.52	16.89	16.5
C (AT)	18500	17000	14150	12750	11500
ε_{0a}	0.00344	0.0034	0.0025	0.0019	0.0020
ε_{max}	0.0005	0.0011	0.0024	0.0011	0.0023
C_{a1}	53.3	60.0	71.39	45.16	44.35
C_{a2}	8.55	20.0	28.28	8.45	12.25

Curve fitting results for the Oxford #4 sample are shown in Fig. 35. Measured data lie between curves obtained from the Perfect Current Transfer model (red line) and the No Current Transfer model (blue line). The thick solid purple line was obtained by taking account of the neutral axis shift, current transfer length, filament breakage and uniaxial strain releasing, in order to fit the experimental data. The neutral axis shift, the current transfer length, the breakage and the thermally induced strain release used for the fittings are shown as a function of the bending strain in Fig. 36. Three dotted purple lines in Fig. 35 show recovery curves of the critical currents after the peak bendings of 0.42%, 0.49% and 0.56%, respectively. The recovered critical currents at zero bending agree well with the experimental results. The Oxford wire sample showed significant irreversible permanent degradation, which could be explained with 2% filament breakage at 0.56% bending strain.

Fig. 37 shows the curve fitting results of a Luvata wire sample, which were obtained with the four effects shown in Fig. 38. The sharp decrease of the critical current above 0.45% bendings was reflected by the sharp increase of the current transfer length. Permanent degradation of the Luvata sample was negligible, implying an absence of filament breakage.

Fig. 39 shows the curve fitting results of an EU EAS wire sample, which were obtained with the four effects shown in Fig. 40. The EAS wire sample showed very small bending effects. The critical current increases slightly with increasing bending strains. This probably is the result of neutral axis shifts.

Fig. 41 shows the curve fitting results of an EU EM-LMI wire sample, which were obtained with the four effects shown in Fig. 42. The internal tin EM-LMI sample showed bending effects as large as other internal tin wires of Oxford and Luvata wires. Permanent degradation of this wire was small, similar to the Luvata wire.

Fig. 43 shows the curve fitting results of a Furukawa wire sample, which were obtained with the four effects shown in Fig. 44. The 1% increase of the critical current for the Furukawa wire sample at 0.3% peak bending can be simulated by assuming a 70 μm shift of the neutral axis.
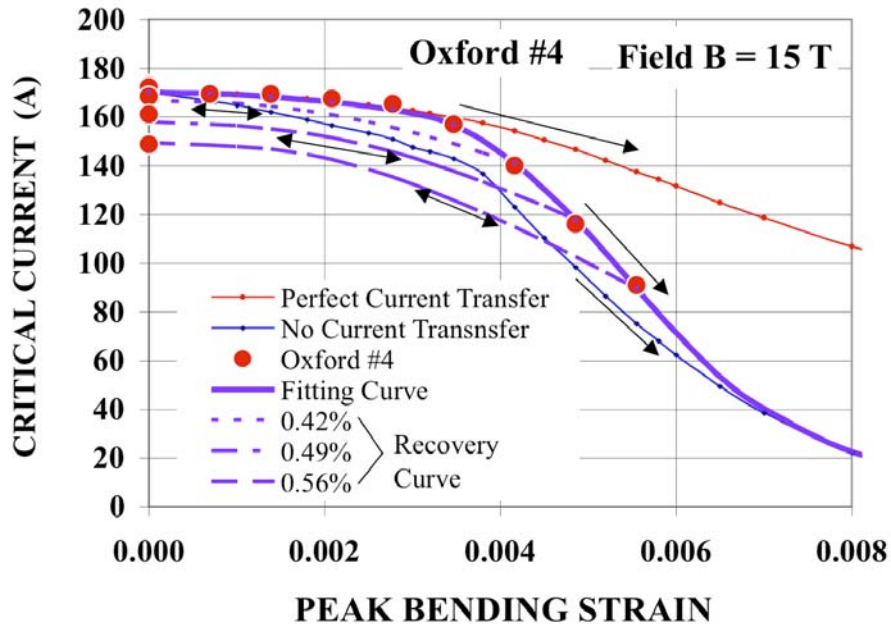
Fig. 35 Curve fittings of the critical currents measured for Oxford wire (red solid circles). Lines are obtained from model calculations: Fine red and blue lines are for perfect current transfer and no current transfer models, respectively. Measured results fit a thick solid purple line which was obtained from the newly developed model. The dotted lines show recovery curves of the critical currents after the peak filament bending strains of 0.42%, 0.49% and 0.56%. The recovered critical currents at zero bending agree well with the experimental results.
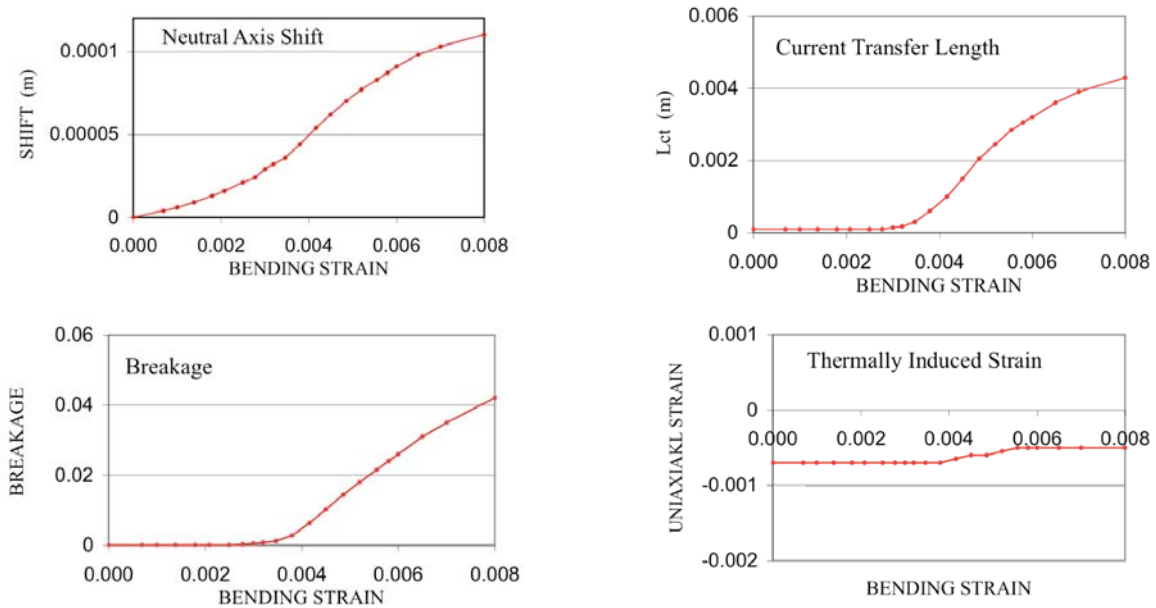

Fig. 36 Estimated behaviors of the neutral axis shift, the current transfer length, the breakage and the thermally induced strain release for Oxford wire as a function of the bending strain.
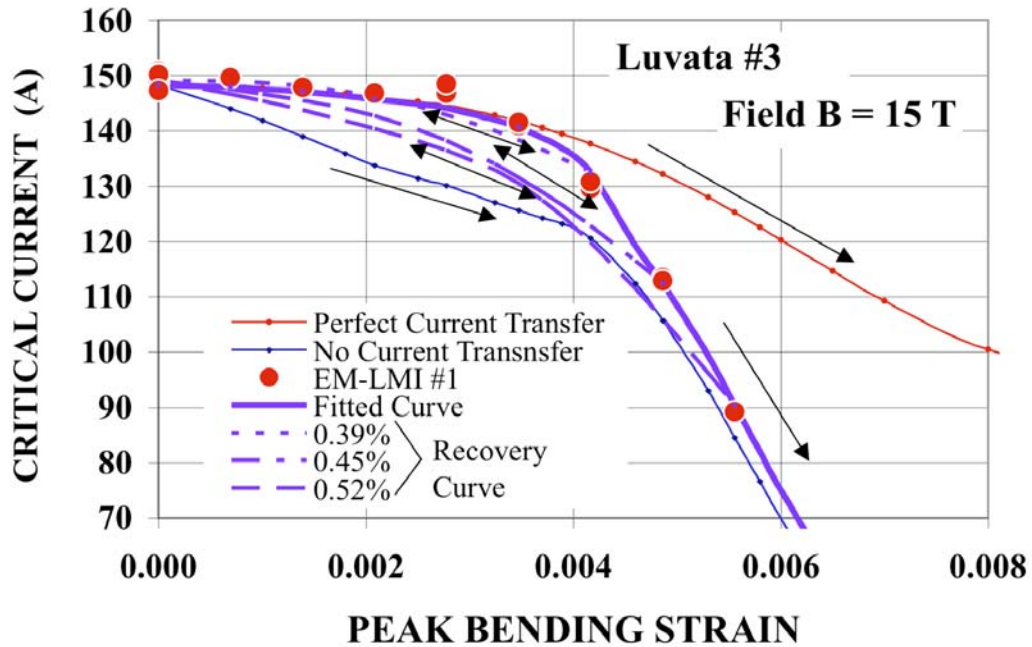
Fig. 37 Curve fittings of the critical currents measured for Luvata wire (red solid circles). Lines are obtained from model calculations: Fine red and blue lines are for perfect current transfer and no current transfer models, respectively. Measured results fit a thick solid purple line which was obtained from the newly developed model. Three dotted lines show recovery curves of the critical currents after the given bending strains.
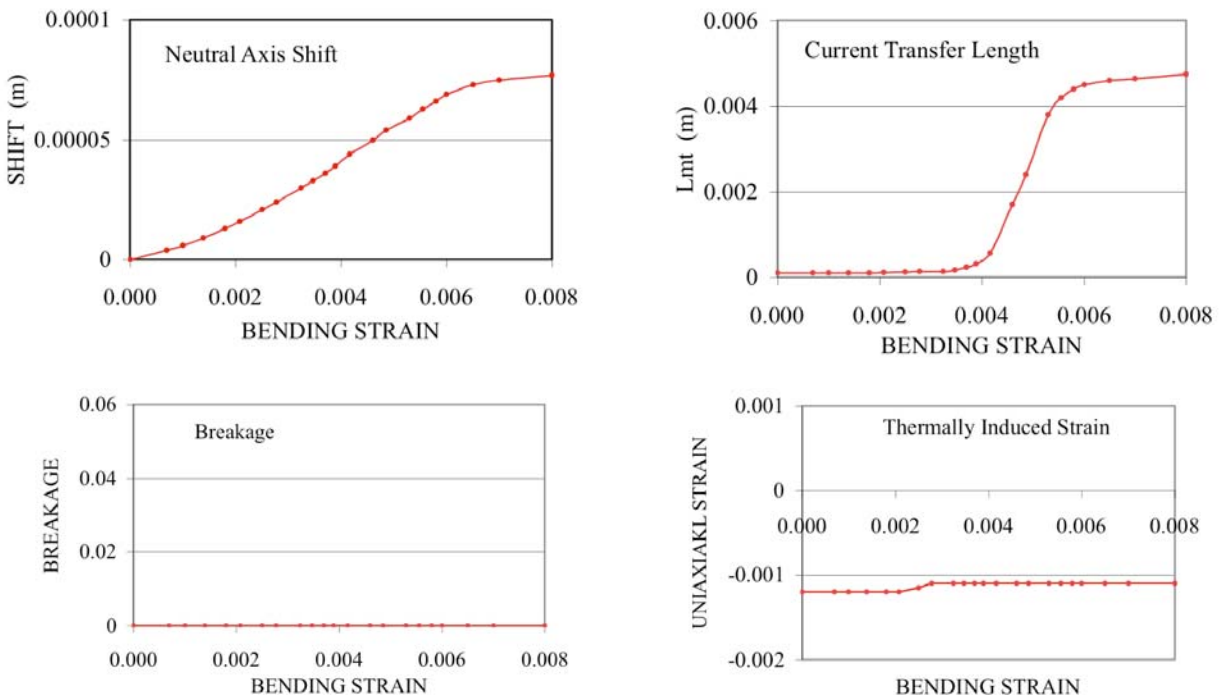

Fig. 38 Estimated behaviors of the neutral axis shift, the current transfer length, the breakage and the thermally induced strain release for Luvata wire as a function of the bending strain.
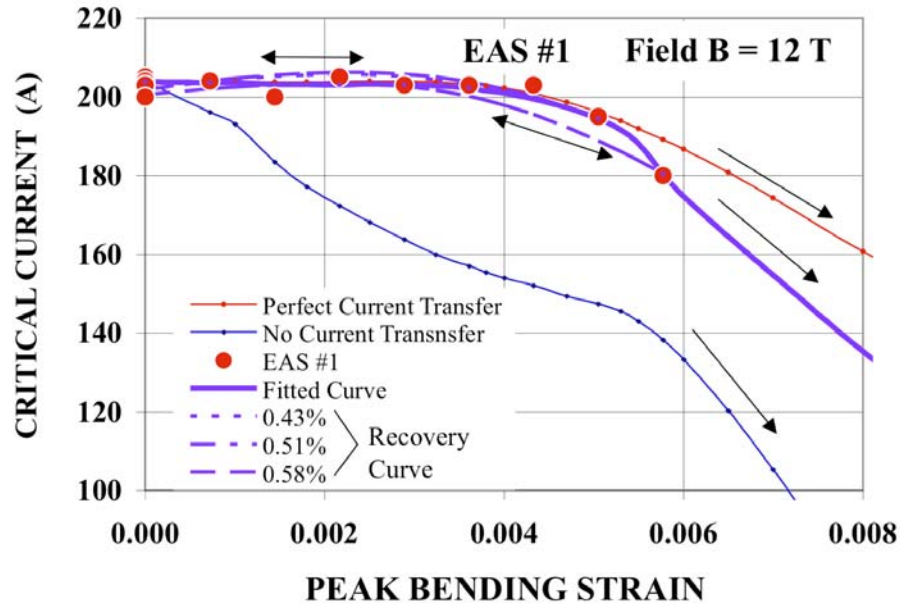
31

Fig. 39 Curve fittings of the critical currents measured for EU EAS wire (red solid circles). Lines are obtained from model calculations: Fine red and blue lines are for perfect current transfer and no current transfer models, respectively. Measured results fit a thick solid purple line which was obtained from the newly developed model. Three dotted lines show recovery curves of the critical currents after the given bending strains.

Fig. 40 Estimated behaviors of the neutral axis shift, the current transfer length, the breakage and the thermally induced strain release for EU EAS wire as a function of the bending strain.

Fig. 41 Curve fittings of the critical currents measured for EU EM-LMI wire (red solid circles). Lines are obtained from mode calculations: Fine red and blue lines are for perfect current transfer and no current transfer models, respectively. Measured results fit a thick solid purple line which was obtained from the newly developed model. Three dotted lines show recovery curves of the critical currents after the given bending strains.
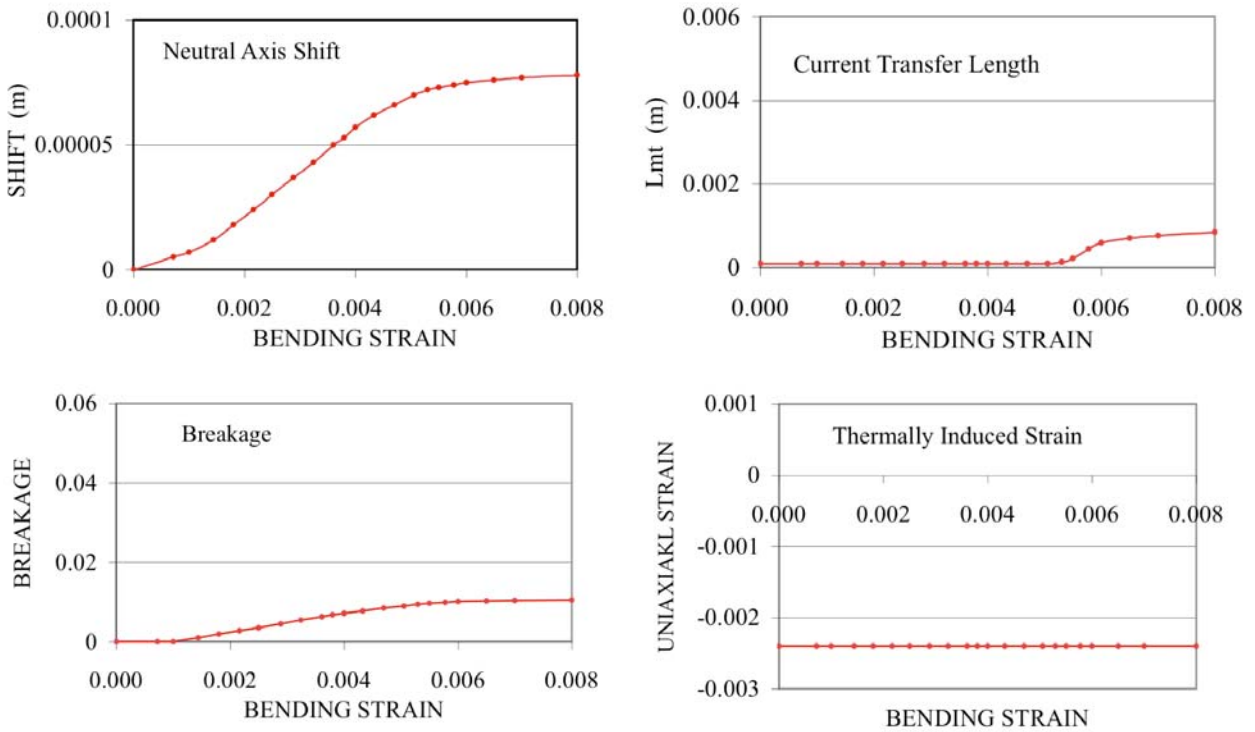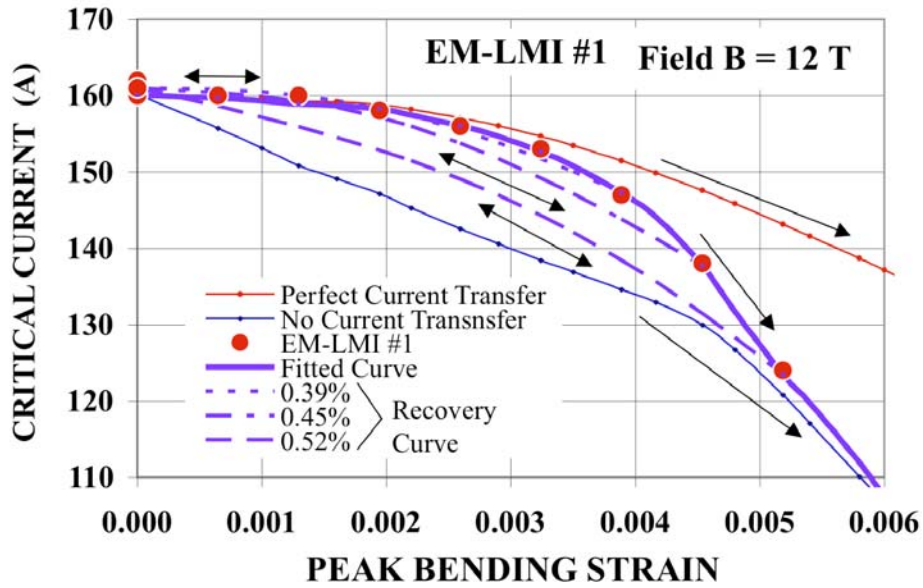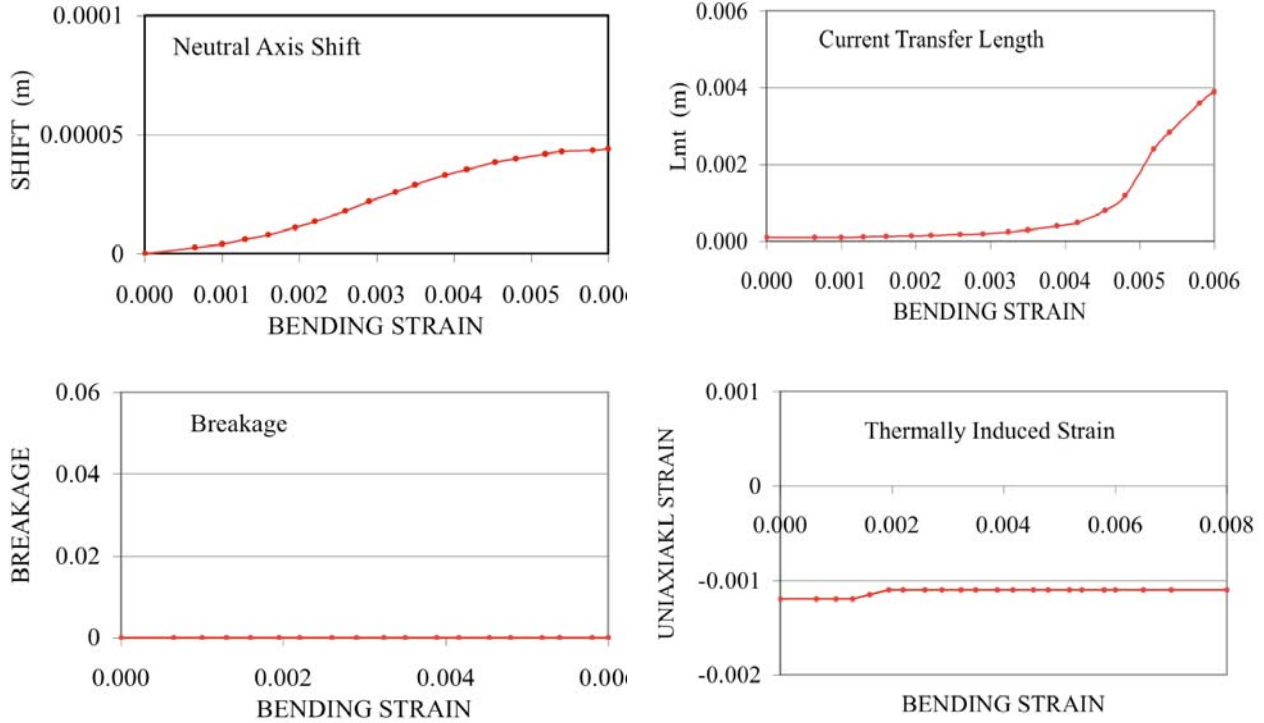

Fig. 42 Estimated behaviors of the neutral axis shift, the current transfer length, the breakage and the thermally induced strain release for EU EM-LMI wire as a function of the bending strain.
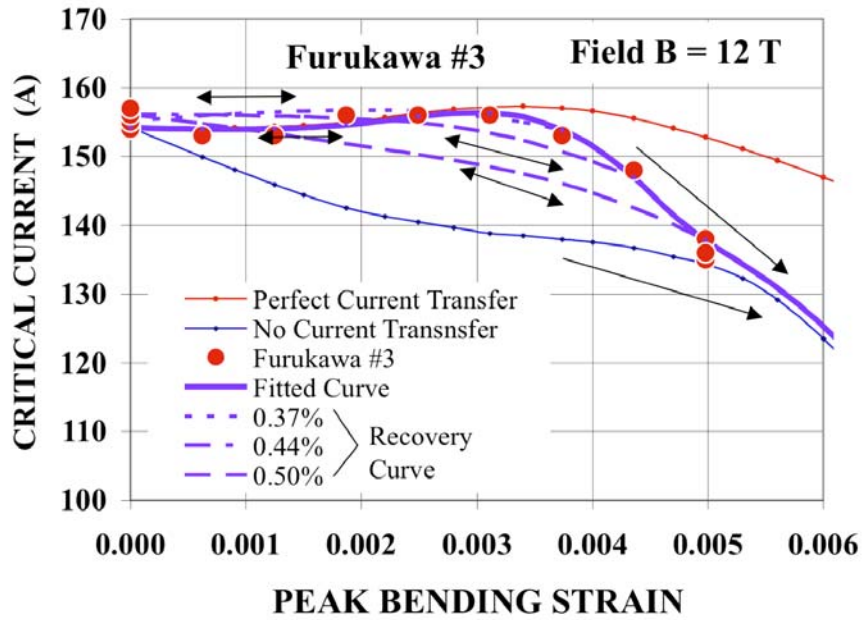
Fig. 43 Ic vs. peak bending strain results measured for Furukawa wire (red solid circles). Lines are obtained from model calculations: Fine red and blue lines are for perfect current transfer and no current transfer models, respectively. Measured results fit a solid purple line which was obtained from the newly developed model. Three dotted lines show recovery curves of the critical currents after the given bendings of 0.37%, 0.44% and 0.50%. The maximum of the critical currents at about 0.3% peak bending and also the recovered critical currents at zero bending agree well with the experimental results.
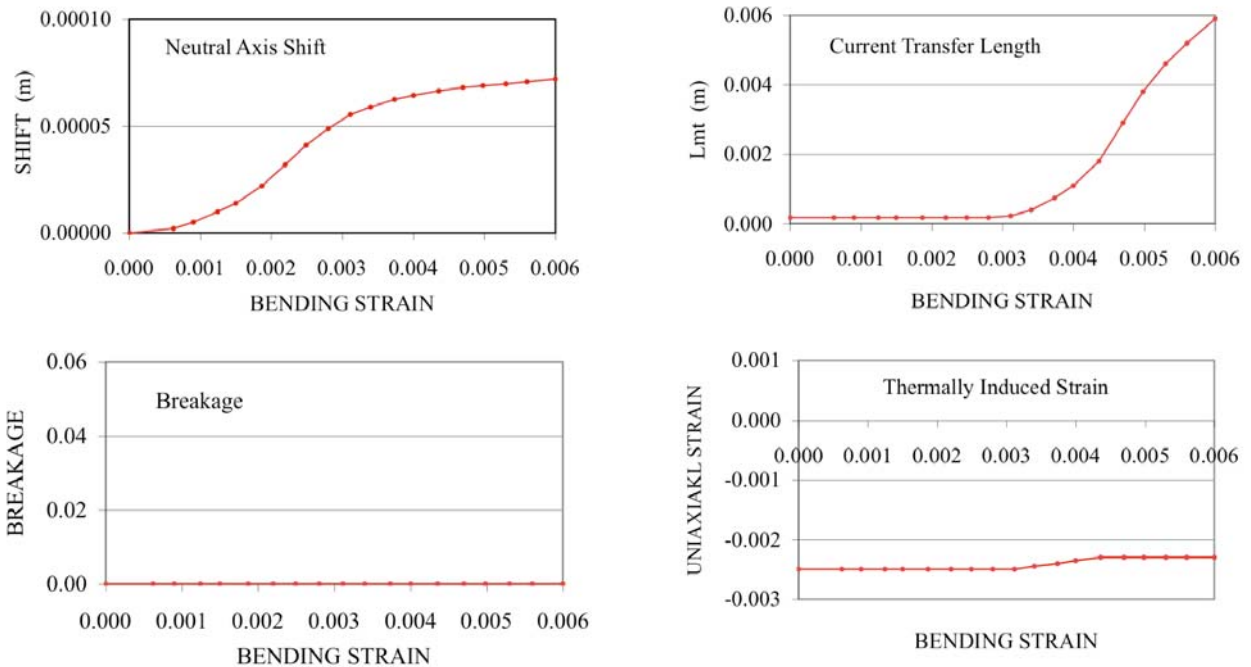

Fig. 44 Estimated behaviors of the neutral axis shift, the current transfer length, the breakage and the thermally induced strain release for Furukawa wire as a function of the bending strain.

The current transfer lengths obtained from data fittings are plotted as a function of the square root of the n-values in Fig 45. The EAS results were not included in this figure since the data were very limited. It has been found that the current transfer length L_{ct} is seen to have a linear relationship with $1/\sqrt{n}$, even though L_{ct} does not exactly proportional to $1/\sqrt{n}$ as it is predicted from Eq. (18) [11],
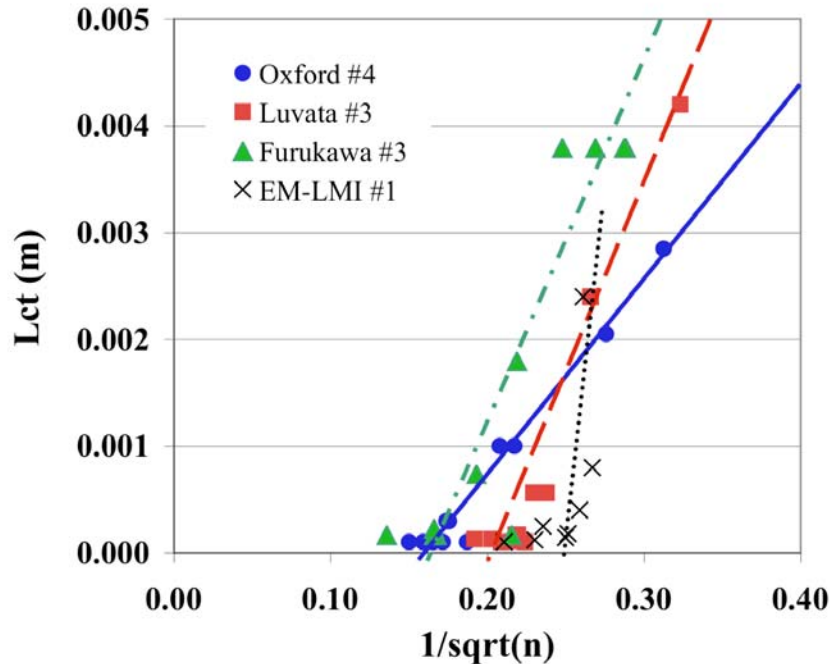

Fig. 45 Current transfer lengths obtained from data fittings as a function of square root of n-values.

The resulted parameters of the neutral axis shift, current transfer length, breakage and thermally induced strain might not be unique determinations. However, each of them had very different contribution to the critical currents, so that the four parameters were relatively easily determined. The parameters of the critical current scaling law for the test wires have not yet been established. The parameters used would be not determined definitively. However the results of the model analyses are not strongly affected by modest changes of the parameters.

The calculated neutral axis shifts for all of the samples were quite large. Further investigations of the mechanical dynamics of the superconducting matrixes during bending are recommended. The recovery behavior of the critical currents after applying bending is especially useful to understanding the effects of bending on the critical currents.

6. Conclusions

The critical currents of the internal tin wires were degraded at 0.8% nominal bending strains by 47% for Oxford wire, 40% for Luvata wire and 30% for EM-LMI wires. Higher current density

wire such as the Oxford wire seems to degrade more than lower current density wires. On the other hand with the 0.8% nominal bending, bronze wires of Furukawa and EAS both degraded by only about 10%. After 0.8% bending, Oxford, Luvata and ESA wires showed 13%, 1.3% and 2% irreversible permanent degradation of their initial critical current values, respectively. However, the critical currents of EM-LMI and Furukawa wires were slightly increased gradually at zero bending strain after each bending cycle. It was found that the Furukawa wire showed clear improvements of the critical currents at the peak bendings of around 0.3%.

The experimental behaviors of the critical currents due to pure bendings have been evaluated with the four effects of neutral axis shift, current transfer length, filament breakage and uniaxial strain release. The neutral axis shift increases the critical current under small bending strains (~0.3%), but does not change the critical current at zero bending state. The current transfer length reduces the critical current with regard to the ratio of the current transfer length and the twist pitch length. The current transfer length is a function of the n-value of the superconductor and the transverse resistance of the matrix. A strand having a longer twist pitch has a smaller effect due to the current transfer length. Longer strand twist pitch is desired although it is typically harmful for AC coupling losses. The filament breakage reflects an irreversible permanent degradation. The filament breakage could result in significant degradation for a strand having a long current transfer length (short twist pitch). The uniaxial strain release (reduction of thermally induced strain) causes enhancement of the critical current.

Better understanding of the bending behavior of Nb_3Sn wires has been obtained by using a newly developed integrated model that accounts for neutral axis shift, current transfer length, mechanical filament breakage and uniaxial strain release. However, further investigations of both electrical and mechanical properties of superconducting wires under pure bending are required.

Acknowledgements

References

[1] D.L. Harris, A.A Allegritti, M. Takayasu, and J.V. Minervini, "Pure bending strand test of high performance Nb_3Sn wires," Adv. Cryo. Eng., 54, Plenum, N.Y., 341-348, 2008.
[2] D.L. Harris, "Characterization of Nb3Sn superconducting strand under pure bending," MIT Mechanical Engineering Masters Thesis, 2005.
[3] A. Allegritti, "Development and experimental test of a device for the measurements of the critical current of superconducting strands under pure bending conditions," University of Bologna, Department of Mechanical Engineering, Italy, 2006.

[4] W. Goldacker, S.I. Schlachter, R. Nast, H. Reiner, S. Zimmer, H. Kiesel, and A. Nyilas, "Bending strain investigation on BSCCO(2223) tapes at 77K applying a new bending technique," Advances in Cryogenic Engineering, 48, 469-476, 2002.

[5] L. Bottura, 2.4.2008, "Jc(B,T,ε) Parameterization for ITER Nb3Sn Production," CERN-ITER collaboration report, Version 2, April 2, 2008.

[6] J.W. Ekin, "Strain Scaling law and the prediction of uniaxial and bending strain effects in multifilamentary superconductors," in *Filamentary A15 Superconductors*, Proceedings of the tropical conference on A15 superconductors, Ed by M. Suenaga and A. Clark, Plenum Press, New York, 187-203, 1980.

[7] N. Mitchell, "Mechanical and magnetic load effects in Nb3sn cable-in-conduit conductors," Cryogenics, 43, 255-270, 2003.

[8] A. Nijhuis and Y. Ilyin, "transverse load optimization in Nb3Sn CICC design; influence of cabling, void fraction and strand stiffness," Supercon. Sci. Technol. 19, 945-962, 2006.

[9] A. Nijhuis, Y. Ilyin, W.A.J. Wessel and W. Abbas, "Critical current and strand stiffness of three types of Nb3Sn strand subjected to spatial periodic bending," Supercon. Sci. Technol. 19, 1136-1145, 2006.

[10] N. Koizumi, Y. Nunoya, and K. Okuno, "A new model to simulate critical current degradation of a large CICC by taking into account strand bending," IEEE Trans. Appl. Supercond. 831-834, 2006.

[11] K. Kaiho, T.S. Luhman, M. Suenaga, W.B. Sampson, "Effects of bending on the superconducting critical current density of monofilamentary Nb3Sn wires," Appl. Phys. Lett. 36, 223-225, 1980.

[12] Y. Kubo and T. Ozawa, "Derivation of Ic degradation rate for reacted Nb_3Sn wires under applied bending and tensile strains," Cryogenic Engineering, Journal of the Cryogenic Society of Japan in Japanese, 37, 68-76, 2002.

[13] M.C. Jewell, P.J. Lee and D.C. Larbalestier, "The influence of Nb3Sn strand geometry on filament breakage under bend strain as revealed by metallography," Supercond Sci Technol, 16, 1005-1011, 2003.

[14] K. Miyoshi, S. Awaji, H. Oguro, G. Nishijima, and K. Watanabe, "Ic enhancement effect in Nb3Sn Coils fabricated by the react-and-wind method," Adv. Cryo. Eng., 52, Plenum, N.Y., 536-543, 2006

[15] J. Ekin, "Current transfer in multifilamentary superconductors. I. Theory," J. Appl. phys. 49, 3406-3409, 1978.

[16] J. Ekin and A.F. Clark, "Current transfer in multifilamentary superconductors. II. Experimental results," J. Appl. phys. 49, 3410-3412, 1978.

[17] A. Nijhuis, "A solution for transverse load degradation in ITER Nb_3Sn CICCs: verification of cabling effect on Lorentz force response," Supercond Sci Technol, 21, 1-15, 2008.

[18] Y. Ilyin, A. Nijhuis and E. Krooshoop, "Scaling law for the strain dependence of the critical current in an advanced ITER Nb3Sn strand," Supercond. Sci. Technol. 20, 186–191, 2007.

[19] D.M.J. Taylor and D.P. Hampshire, "The scaling law for the strain dependence of the critical current density in Nb3Sn superconducting wires," Supercond. Sci. Technol. 18, S241–S252, 2005.